LUND
UNIVERSITY

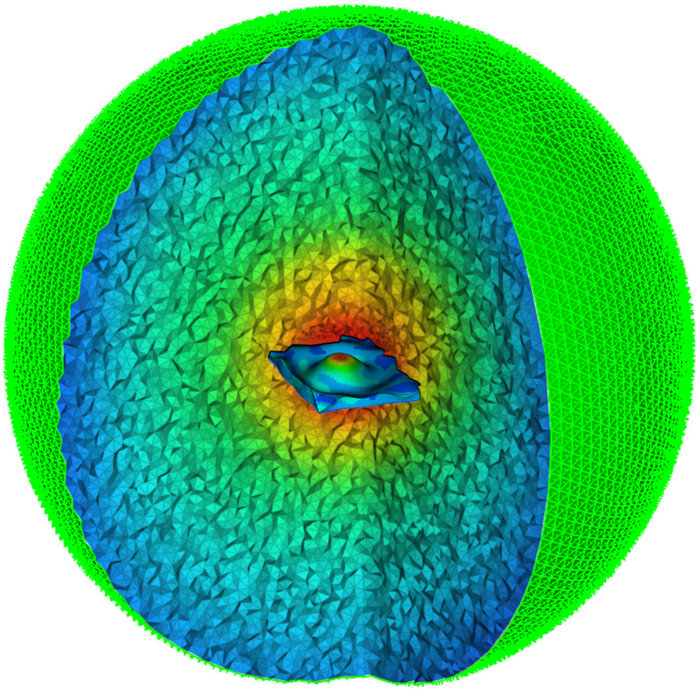

STRUCTURE–ACOUSTIC INTERACTION BETWEEN VEHICLE FLOOR PANELS AND CARPETS

Numerical Simulations and Measurements

AYA KARIM & JESPER BRINDHAG

Structural
Mechanics

Master's Dissertation

DEPARTMENT OF CONSTRUCTION SCIENCES
DIVISION OF STRUCTURAL MECHANICS
ISRN LUTVDG/TVSM--21/5251--SE (1-69) | ISSN 0281-6679
MASTER'S DISSERTATION

STRUCTURE–ACOUSTIC INTERACTION BETWEEN VEHICLE FLOOR PANELS AND CARPETS

Numerical Simulations and Measurements

AYA KARIM & JESPER BRINDHAG

Supervisors: Dr **OLA FLODÉN**, Division of Structural Mechanics, LTH,
and **LILLY MA**, MSc, Driving Dynamics & NVH Centre, Volvo Cars.
Examiner: **PETER PERSSON**, Associate Professor, Division of Structural Mechanics, LTH.

Copyright © 2021 Division of Structural Mechanics,
Faculty of Engineering LTH, Lund University, Sweden.
Printed by V-husets tryckeri LTH, Lund, Sweden, July 2021 *(Pl).*

For information, address:
Division of Structural Mechanics,
Faculty of Engineering LTH, Lund University, Box 118, SE-221 00 Lund, Sweden.
Homepage: www.byggmek.lth.se

Acknowledgements

This Master's dissertation was carried out for the Division of Structural Mechanics at the Faculty of Engineering of Lund University, LTH, in cooperation with Volvo Cars; and concludes five years of studying civil engineering, with a Master's specialization in structural engineering. We would like to start off by thanking our supervisor at Volvo Cars, Lilly Ma, for keeping up with our work and for always being available to us when needed, even outside of working hours. We would like to thank Dr Lars Nordström from Volvo Cars for his input; and extend our thanks to Volvo Cars for making this dissertation possible, and for welcoming us at their headquarters in Gothenburg at the beginning of our work. We would also like to express our sincere thanks to our supervisor at LTH, Dr Ola Flodén, for his enthusiasm, expertise and guidance throughout the work. Lastly, we would like to thank each other for the great company the past two years.

On a personal note, I would like to show my gratitude to my parents, Naji Karim and Huda Murtada, and my brothers, Dhia and Amir, for their continuous encouragement. Special thanks dedicated to my mother for her emotional support and unconditional love on days where my motivation was not at its highest during those five years.

Aya Karim, Malmö, 2021

I would like to thank my son, Caspian Brindhag, for being the happiest little man and for being the motivation I needed during these five years of study.

Jesper Brindhag, Åkarp, 2021

Abstract

An attribute that is highly valued amongst vehicle customers is low interior-noise levels when a vehicle is in use. Much of the interior-noise is believed to stem from the vibrations of floor panels in vehicles. Sources to these vibrations can be, for instance, e-motors, engines and road–tire interaction, which in turn is translated into disturbing noise inside the cabin. Interior carpets placed on the floor panels dampen the vibrations and reduce the noise transmission and radiation from the floor panels. The interior carpets in vehicles are usually composed of a light foam material covered by a heavy rubber layer on top, called heavy layer. Due to the different material layers and mechanical properties in such floor panel–carpet setups, the dynamic interaction and structure–acoustic interaction between the layers is complex. The layers vibrate with different, and sometimes conflicting, amplitudes and patterns at different frequencies. This dissertation investigates the structure–acoustic interaction in floor panel–carpet setups, with the dynamic interaction as a starting point, in order to increase the knowledge regarding noise radiation from the setups. Different modelling approaches with increasing complexity for the carpet are considered in order to give guidelines and recommendations for finite element modelling that is able to accurately represent the true behaviour of floor panel–carpet setups at different frequencies. This dissertation also presents an experimental testing that was conducted on a real floor panel–carpet to verify the findings.

It was found that a simplified model in which only the mass of the carpet was considered, and distributed evenly on the floor panel, was sufficient to represent the vibration response and acoustic radiation of the floor panel–carpet setup at low frequencies. It was further established that at higher frequencies, geometrical and structural aspects of the carpet are essential to define in order to predict the behaviour with sufficient accuracy. When evaluating the vibration response of the floor panel–carpet setup at higher frequencies, it was found that a model in which the carpet was assigned linear elastic material properties gave satisfactory results in relation to a more advanced model in which the carpet was assigned porous elastic material properties based on Biot's theory. Further, when evaluating the acoustic radiation from the floor panel–carpet setup at higher frequencies, it was deemed necessary to acknowledge the air within the pores of the foam material of the carpet. Lastly, it was concluded that the main contributor to the disturbing interior-noise stemming from the floor panel–carpet setup, can be summarized as follows;

- Low frequencies: Floor panel and carpet radiate noise as a solid unit
- Mid frequencies: Heavy layer of the carpet dominates the radiation
- High frequencies: Floor panel dominates the radiation

Contents

1 Introduction **1**
1.1 Background 1
1.2 Aim and Objective 2
1.3 Methodology 2
1.4 Limitations 2
1.5 Disposition 3

2 Structural Dynamic Analysis **5**
2.1 Equations of Motion 5
2.2 Eigenvalue Analysis 6
2.3 Forced Harmonic Response 6
2.4 Modal Truncation 7
2.5 Frequency Response Function 8
2.6 Damping 8

3 Structural Acoustic Analysis **11**
3.1 Continuum and Finite Element Formulation 11
  3.1.1 Structural Domain 11
  3.1.2 Acoustic Fluid Domain 13
  3.1.3 Coupling of Domains 15
  3.1.4 Biot’s Theory 16
3.2 Equivalent Radiated Power 16
3.3 Noise Transfer Function 17

4 Example Case of Floor Panel and Carpet **19**
4.1 Software and Finite Element Solvers 19
4.2 Geometry and Materials 20
4.3 Dynamic Excitation and Boundary Conditions 22
4.4 Finite Element Modelling of Panel and Carpet 23
  4.4.1 Non-Structural Mass Model 23
  4.4.2 Linear Elastic Material Model 24
  4.4.3 Porous Elastic Material Model 24
4.5 Implementation of External Acoustic Domain 25

5 Simulation of Vibration Response 27
5.1 Vibration Response 27
5.2 Operating Deflection Shape 29
5.3 Convergence Studies for Finite Element Settings 32
5.3.1 Direct and Modal Analysis 32
5.3.2 Mesh Criteria 33
5.4 Sensitivity Studies for Porous Elastic Material Model 34
5.4.1 Panel–Carpet Coupling 34
5.4.2 Panel Thickness 35
5.4.3 Material Damping 35
5.4.4 Young's modulus of Heavy Layer 38
5.4.5 Biot Parameters 38

6 Simulation of Acoustic Radiation 43
6.1 Acoustic Radiation 43
6.2 Structure–Fluid Coupling in Porous Elastic Material Approach 46
6.3 Noise Radiation Process 47

7 Experimental Testing and Correlation 51
7.1 Geometry and Material of Test Sample 51
7.2 Experimental Setup and Methodology 51
7.3 Measurement Results 54
7.4 Correlation to Numerical Results 55

8 Conclusions and Discussion 59
8.1 Vibration Response 59
8.1.1 Frequency–Dependent Behaviour 59
8.1.2 Modelling Choice of Carpet 59
8.2 Acoustic Radiation 60
8.2.1 Modelling Choice of Carpet 60
8.2.2 Governing Physical Phenomena 60
8.3 Experimental Testing and Correlation 61
8.4 Proposals for Future Work 61

Bibliography 61

Appendices 65
A ERP Deviation in Porous Elastic Material Approach I
B Measurement Results III
B.1 Accelerations III
B.2 Acoustic Pressure IV
B.3 Coherence V

List of Acronyms

DoF	Degree(s) of Freedom
ERP	Equivalent Radiated Power
FE	Finite Element
FRF	Frequency Response Function
HL	Heavy Layer
LE	Linear Elastic
MDoF	Multi Degrees of Freedom
NSM	Non-Structural Mass
NTF	Noise Transfer Function
NVH	Noise, Vibration, Harshness
ODS	Operating Deflection Shape
PEM	Porous Elastic Material
SDoF	Single Degree of Freedom
TCL	Thermal Characteristic Length
VCL	Viscous Characteristic Length

Chapter 1

Introduction

The following is an introductory chapter that gives the reader an overview of the issue that has led up to the formulation of this Master's dissertation. The purpose, aim and objective of the dissertation, as well as the approach through which the dissertation has been executed, are explained. Factors that have limited the scope of the work are mentioned. Lastly, a short description reviewing the content of each chapter in this dissertation is presented to make it easier for the reader to navigate through the work.

1.1 Background

Of great importance when developing a car model is the noise, vibration and harshness (NVH) attributes as they directly affect the user experience and often are seen as an indicator of overall vehicle quality. An attribute that falls within the NVH definition, and that is especially desired and highly valued amongst customers, is low interior-noise levels when the vehicle is in use. In order to achieve better NVH performance, especially for premium segment cars, noise transmitted into the cabin of the vehicle disturbing the overall user experience, needs to be reduced. Tire–road interaction, engines and e-motors are all examples of sources from which disturbing noise arises. The disturbing noise is then transmitted into the cabin either through air, called airborne noise, or as structural vibrations through panels surrounding the cabin, called structure–borne noise. Mitigation of the latter should be considered in all steps of the transmission chain, i.e.

1. at the source
2. in the vibration transmission to the panels
3. in the noise radiation from the panels
4. through acoustics absorption

A significant portion of the structure–borne interior-noise is suspected to stem from the floor panels of a vehicle. Such floor panels are normally made of metal covered by interior carpets which dampen the noise transmission and radiation. The interior carpets often consist of a light foam material over which a heavy rubber layer is applied. Interior floor carpets fall into what is defined as a trim component. Trim components are the dampers and insulators in a vehicle and are usually made of porous material providing the absorbing effect. In product development, trim components are often either neglected or treated as a non-structural mass when modelling a whole vehicle body. The vibration interaction in such panel–carpet setups has formerly been investigated, why the dynamic behaviour of the coupled system is recognized for different frequency ranges [1] [2] [3] [4]. However, the structure–acoustic interaction between the panel–carpet setup and surrounding air in the cabin is rather unclear and in need of more research.

1.2 Aim and Objective

Through more accurate predictions of structure–borne interior-noise in vehicles, one may establish more informed design decisions when it comes to floor panel–carpet setups. The aim of this Master's dissertation is to improve the knowledge regarding the structure–acoustic interaction between vehicle floor panels and interior floor carpets. This dissertation aims to develop and compare calculation models for floor panel–carpet setups that are able to accurately represent the trim component and its impact on the structure–acoustic performance. The objective is to analyze and provide a basic understanding of the disturbing noise radiation process from floor panel-carpet setups, and the governing physical phenomena.

1.3 Methodology

This dissertation regards an example case of a simplified floor panel–carpet setup with flat components. The studied floor panel–carpet setup is based on a vehicle produced by Volvo Cars, and is described in detail in Chapter 4. The work was conducted with the use of the finite element (FE) method, in which numerical analyses were performed concerning frequencies that are most critical for structure–borne noise. The work can be summarized according to the following:

- Evaluate the dynamic response of a floor panel–carpet setup, using three different modelling approaches with increasing complexity for the carpet in the setup.
- With the dynamic response as a starting point, investigate the acoustic radiation from the floor panel–carpet setup into an infinite acoustic air domain.
- Investigate the dynamic and acoustic response of the floor panel–carpet setup in order to identify governing physical phenomena, e.g. by examining different ways of modelling the structure–acoustic coupling between the studied setup and the surrounding air domain.
- Correlate and verify numerically obtained results with experimental testing of a real floor panel–carpet setup.

1.4 Limitations

This dissertation only regards structure–borne noise stemming from the vibrations of floor panels in vehicles. Only a simplified floor panel and interior carpet setup was investigated. The studied setup has flat components and is based on a vehicle produced by Volvo Cars. The studied frequency range for the dynamic interaction of the components of the setup was limited to 0 – 1000 Hz, whereas the frequency range for the structure–acoustic interaction of the components was limited to 100 – 600 Hz. The vibration response and acoustic radiation were evaluated due to a dynamic unit point load in transverse direction, by means of equivalent radiated power and acoustic pressure, respectively. Three modelling approaches for the carpet in the setup were considered: 1) by only regarding the mass of the carpet, 2) by assigning the carpet linear elastic material properties, and 3) by assigning the carpet porous elastic material properties.

1.5 Disposition

This dissertation contains eight chapters. The following section presents an overview of each of the chapters for easier navigation through the work.

Chapter 2: Structural Dynamic Analysis

This is a chapter of theoretical background that introduces the reader to basic concepts regarding linear structural dynamic analyses, e.g. equations of motions, forced harmonic response and frequency response function.

Chapter 3: Structural Acoustic Analysis

This is a chapter of theoretical background that introduces the reader to acoustic concepts that are of relevance to the work done in this dissertation. The chapter focuses on FE derivation of the governing equations in the structural domain and acoustic fluid domain when performing structural acoustic analyses.

Chapter 4: Example Case of Floor Panel and Carpet

This chapter presents the example case studied in this dissertation. The example case regards a simplified floor panel–carpet setup with flat components. The dimensions, material parameters and conditions of the studied setup are presented in this chapter. Further, the FE software used and FE modelling of the studied setup are described.

Chapter 5: Simulation of Vibration Response

The vibration response of the example case described in Chapter 4 is simulated and evaluated in this chapter. Discussions regarding the vibration behaviour of the studied panel–carpet setup, in relation to the used modelling approaches are further presented. A number of convergence studies motivating FE choices, as well as sensitivity analyses regarding uncertain input parameters are conducted and reviewed.

Chapter 6: Simulation of Acoustic Radiation

With an implemented acoustic fluid domain, the acoustic radiation from the studied panel–carpet setup is presented and discussed. Hypotheses regarding main contributors of the structure–borne noise in different frequency ranges are further investigated by comparing the acoustic radiation to the vibration response presented in Chapter 5.

Chapter 7: Experimental Testing and Correlation

This chapter contains experimental testing conducted on a flat floor panel–carpet setup, that was provided by Volvo Cars. The vibration response and acoustic radiation is evaluated using accelerometers attached to the suspended setup, and microphones placed nearby the setup. Correlation and validation of observations and conclusions drawn previously are confirmed.

Chapter 8: Conclusions and Discussions

This final chapter presents a summary of the conclusions and discussions made throughout this dissertation. Proposals for future work are suggested.

Chapter 2

Structural Dynamic Analysis

Structural dynamics covers the study, by theoretical, numerical or experimental means, of structural behaviour of a physical system subjected to dynamic loading. A dynamic load is a load that varies with time, and as a result induces time-dependent response in the loaded system. Oftentimes, the said response is translated into the frequency domain. The following chapter introduces the reader to the basics of structural dynamics, and is limited to linear dynamic analyses.

2.1 Equations of Motion

A relation that describes the state at which dynamic equilibrium is attained for a physical system in motion is called the equation of motion. In its most simplified form, the movement of a structure can be described by a single degree of freedom (SDoF). When exciting a SDoF system with an external dynamic load $p(t)$, the equation of motion takes the form

$$m\ddot{u} + c\dot{u} + ku = p(t)\,, \tag{2.1}$$

indicating that the internal response of the system originates from three different sources; namely its inertia mass m, its damping c and its stiffness k. The variables u, $\dot{u}$ and $\ddot{u}$ stand for displacement, velocity and acceleration, respectively, and are all a function of time t.

When going over to a multi degree of freedom (MDoF) system, Eq. (2.1) becomes a set of equations according to

$$\mathbf{M}\ddot{\mathbf{u}} + \mathbf{C}\dot{\mathbf{u}} + \mathbf{K}\mathbf{u} = \mathbf{p}(t)\,, \tag{2.2}$$

where $\mathbf{M}$ is the mass matrix, $\mathbf{C}$ the damping matrix, $\mathbf{K}$ the stiffness matrix and $\mathbf{p}(t)$ the external dynamic force vector. Similarly to before, the variables $\mathbf{u}$, $\dot{\mathbf{u}}$ and $\ddot{\mathbf{u}}$ denote the displacement, velocity and acceleration vectors each [5]. This chapter hereinafter deals with MDoF systems.

2.2 Eigenvalue Analysis

A system can be excited by an initial displacement and/or velocity while the external load is equal to zero. The response is then called the free vibration response, and its equations of motion take the form

$$\mathbf{M}\ddot{\mathbf{u}} + \mathbf{C}\dot{\mathbf{u}} + \mathbf{K}\mathbf{u} = \mathbf{0}\,, \tag{2.3}$$

resulting in a response that decays exponentially with time due to the presence of damping. Although there exists no real system with zero damping, studying the undamped system provides an insight into its vibrational behaviour. Eq. (2.3) when damping is left out becomes

$$\mathbf{M}\ddot{\mathbf{u}} + \mathbf{K}\mathbf{u} = \mathbf{0}\,. \tag{2.4}$$

The above set of second-order differential equations can be solved by assuming harmonic time-dependence for the displacement vector, for instance

$$\mathbf{u} = \boldsymbol{\phi} \sin \omega t\,, \tag{2.5}$$

with $\boldsymbol{\phi}$ being a time-independent vector and ω being the angular frequency. Insertion of (2.5) into Eq. (2.4) yields

$$\left(\mathbf{K} - \omega^2\mathbf{M}\right) \boldsymbol{\phi} = \mathbf{0}\,, \tag{2.6}$$

which is true if $\boldsymbol{\phi} = \mathbf{0}$, or $\det\left(\mathbf{K} - \omega^2\mathbf{M}\right) = \mathbf{0}$. The latter solution is of interest, resulting in

$$\begin{cases} \omega_1,\ \omega_2,\ \dots,\ \omega_n & \text{natural frequencies} \\ \boldsymbol{\phi}_1,\ \boldsymbol{\phi}_2,\ \dots,\ \boldsymbol{\phi}_n & \text{mode shapes, also called eigenmodes} \end{cases}$$

with n being the number of degrees of freedom (DoF) in the system. A natural frequency is a frequency at which the system tends to naturally oscillate when disturbed. An eigenmode refers to the vibrational pattern a system displays when excited at the corresponding natural frequency. By assuming a linear combination of the different modes, which form an orthogonal base, one can express the displacement vector as

$$\mathbf{u}(t) = \sum_{i=1}^{n} \boldsymbol{\phi}_i\, q_i(t) = \boldsymbol{\phi}\, \mathbf{q}(t)\,, \tag{2.7}$$

where $\mathbf{q}(t)$ represents modal coordinates, which similarly to $\mathbf{u}(t)$ depend on initial conditions. This method in which modal vectors are superposed to express the system response is called modal decomposition [5], and is an exact representation of the response.

2.3 Forced Harmonic Response

A dynamic force whose magnitude alters sinusoidally with time is called a harmonic force. A harmonic force can be described by the function

$$\mathbf{p}(t) = \mathbf{p_0}\, e^{i\omega t}\,, \tag{2.8}$$

where $\mathbf{p_0}$ is a time-independent vector defining the complex amplitude of the force at each DoF of the excited system. Insertion of (2.8) into the equations of motion, while considering an undamped system, yields

$$\mathbf{M\ddot{u}} + \mathbf{Ku} = \mathbf{p_0}\, e^{i\omega t}\,. \tag{2.9}$$

Assuming the particular solution

$$\mathbf{u} = \mathbf{u_0}\, e^{i\omega t}\,, \tag{2.10}$$

and inserting it into Eq. (2.9), while cancelling out the mutual term, gives

$$\left(\mathbf{K} - \omega^2\mathbf{M}\right)\mathbf{u_0} = \mathbf{p_0}\,, \tag{2.11}$$

where similarly to $\mathbf{p_0}$, $\mathbf{u_0}$ is a time-independent vector defining the complex amplitude of the displacement at each DoF. Eq. (2.9), and consequently (2.11), are examples of a coupled system, in which the set of equations can not be solved independently. For computational efficiency, one could make use of modal decomposition in order to decouple the equations of motion. When uncoupled, Eq. (2.11) takes the form

$$\left(\mathbf{K^{\Phi}} - \omega^2\mathbf{M^{\Phi}}\right)\mathbf{q_0} = \boldsymbol{\phi}^{\intercal}\,\mathbf{p_0}\,, \tag{2.12}$$

in which $\mathbf{K^{\Phi}}$ and $\mathbf{M^{\Phi}}$ denote the generalized stiffness and mass matrices, respectively, and are equal to

$$\mathbf{K^{\Phi}} = \boldsymbol{\phi}^{\intercal}\,\mathbf{K}\,\boldsymbol{\phi}\,, \tag{2.13}$$

$$\mathbf{M^{\Phi}} = \boldsymbol{\phi}^{\intercal}\,\mathbf{M}\,\boldsymbol{\phi}\,.$$

Due to the orthogonality of the modal vectors, the generalized expressions above refer to diagonalized matrices allowing Eq. (2.12) to be solved as a SDoF system, which is the basis for modal frequency response analysis. The inverse of Eq. (2.11) forms the basis for direct frequency response analysis [5].

2.4 Modal Truncation

To further increase computational efficiency, while maintaining sufficient accuracy, one could exclude higher-order modes in a modally decomposed system. This method, known as modal truncation, results in a reduced set of modal coordinates to describe the system, according to

$$\mathbf{u}(t) = \sum_{i=1}^{k} \phi_i\, q_i(t) = \boldsymbol{\phi}\,\mathbf{q}_{\text{reduced}}(t)\,, \tag{2.14}$$

where $k < n$, with n being the number of DoF in the system. While cutting off higher-order modes may lead to possible errors due to simplifying the structural behaviour, it is arguably advantageous as it eliminates errors due to deviations when introducing FE discretisation, which become especially pronounced in higher-order modes [5]. A general rule of thumb is to include modes up to twice the frequency of interest.

2.5 Frequency Response Function

The frequency response function (FRF), denoted by $H(\omega)$ if expressed in rad/s or by $H(f)$ if instead expressed in Hz, is the ratio of output to input of an excited system expressed in the frequency domain. Mathematically speaking, FRF is described by

$$H(f) = \frac{Y(f)}{X(f)}\,, \tag{2.15}$$

where $X(f)$ is the input and $Y(f)$ is the output response of the studied system. In structural dynamic terms, FRF illustrates how the steady-state response of an excited system relates to its sinusoidal input according to

$$H(\omega) = \frac{\mathbf{u_0}}{\mathbf{p_0}}\,, \tag{2.16}$$

for the above denotations, refer back to Section 2.3. The steady-state response is the response a system exhibits after it reaches steady conditions [6]. FRF can be displayed through different formats, one of which is the mobility format. Instead of describing the displacement in relation to the input force as in Eq. (2.16), the mobility FRF relates the obtained velocity to the input force according to

$$H(\omega) = \frac{\mathbf{v_0}}{\mathbf{p_0}}\,. \tag{2.17}$$

This FRF in particular is referred to as the vibration transfer function, and is a popular choice for the automobile industry when evaluating the dynamic response of a system, as numerous physical phenomena are directly proportional to velocity [7].

2.6 Damping

Damping is a complex phenomenon which refers to the dissipation of mechanical energy of a vibrating structure. Energy dissipation can stem from many sources, e.g. material damping, friction in interfaces and energy transfer over domain boundaries. The loss of energy, which reduces the oscillatory response with time, is represented in dynamic analyses by introducing a damping force to the equation of motion of the studied system [5], refer back to Eq. (2.1) and (2.2). The most common damping models are

- Viscous damping, in which the force is proportional to velocity
- Structural damping, in which the force is proportional to displacement
- Coulomb damping, in which the force shows independent behaviour [8]

In structural dynamics, damping matrices $\mathbf{C}$ are usually categorized in terms of classical and non-classical damping. Damping matrices of the former type are advantageous as they are possible to modally diagonalize, allowing MDoF systems to be solved as uncoupled SDoF systems, whereas damping matrices of the latter type are not diagonalizable. Assuming classical damping, Eq. (2.2) when modally decomposed takes the standard form

$$\ddot{q}_n + 2\zeta_n\,\omega_n\,\dot{q}_n + \omega_n^2\,q_n = \frac{P_n(t)}{M_n}\,, \tag{2.18}$$

where the damping ratio ζ_n, natural frequency ω_n and modal load $P_n(t)$ are each given by

$$\zeta_n = \frac{C_n}{2M_n\,\omega_n}\;; \quad \omega_n^2 = \frac{K_n}{M_n}\;; \quad P_n(t) = \boldsymbol{\phi}^{\mathsf{T}}\,\mathbf{p}(t)\,, \tag{2.19}$$

in which M_n, C_n and K_n each denote the diagonal term in the corresponding matrices [5].

Chapter 3

Structural Acoustic Analysis

A vibrating structure that is surrounded by an acoustic fluid is analyzed within the field of structural acoustics. As the name may suggest, structural acoustics involve the interaction of physical phenomena of two different fields – acoustics and structural mechanics. The following chapter starts off with the continuum formulation of the equation of motion governing the structural domain, the wave equation governing the fluid domain, and relations ensuring continuity inbetween. With the continuum formulation as a starting point, FE discretisation is introduced and the FE formulation is derived. Moreover, the chapter sheds light on acoustic concepts such as structure–borne noise, wave propagation and equivalent radiated power. The reader is assumed to have a basic understanding of the FE method.

3.1 Continuum and Finite Element Formulation

A structure–acoustic system is composed of a structure domain Ω_S (structural object) and an acoustic fluid domain Ω_F (liquid or gas carrying acoustic waves). To ensure acoustical coupling of these domains, continuity conditions regarding displacement and pressure at the fluid–structure interface $\partial\,\Omega_{SF}$ need to be defined [9]. In the following derivations, the subscripts S and F are used to denote a quantity in the structural domain and acoustic fluid domain, respectively.

3.1.1 Structural Domain

For a three dimensional structure with continuous mass and made of continuum material, the equation of motion describing the dynamic equilibrium condition takes the differential form

$$\tilde{\nabla}^{\mathsf{T}}\boldsymbol{\sigma}_S + \mathbf{b}_S = \rho_S \frac{\partial^2 \mathbf{u}_S}{\partial t^2}\,, \tag{3.1}$$

where $\tilde{\nabla}$ is a matrix differential operator, $\boldsymbol{\sigma}_S$ is a vector containing all the stress components, $\mathbf{b}_S$ is the body force vector and where the right-hand side of the equation denotes the inertia force in which ρ_S is the mass density, $\mathbf{u}_S$ is the displacement vector and t is time. The differential operator and vector quantities are defined according to

$$\tilde{\nabla}^{\mathsf{T}} = \begin{bmatrix} \frac{\partial}{\partial x} & 0 & 0 & \frac{\partial}{\partial y} & \frac{\partial}{\partial z} & 0 \\ 0 & \frac{\partial}{\partial y} & 0 & \frac{\partial}{\partial x} & 0 & \frac{\partial}{\partial z} \\ 0 & 0 & \frac{\partial}{\partial z} & 0 & \frac{\partial}{\partial x} & \frac{\partial}{\partial y} \end{bmatrix}; \quad \boldsymbol{\sigma}_S = \begin{bmatrix} \sigma_{xx} \\ \sigma_{yy} \\ \sigma_{zz} \\ \sigma_{xy} \\ \sigma_{xz} \\ \sigma_{yz} \end{bmatrix}; \tag{3.2}$$

$$\mathbf{b}_S = \begin{bmatrix} b_x \\ b_y \\ b_z \end{bmatrix}; \quad \mathbf{u}_S = \begin{bmatrix} u_x \\ u_y \\ u_z \end{bmatrix}.$$

To assert the relation between stresses $\boldsymbol{\sigma}_S$ and displacements $\mathbf{u}_S$, the following constitutive relation is adopted assuming linear elasticity

$$\boldsymbol{\sigma}_S = \mathbf{D}_S\, \boldsymbol{\varepsilon}_S\,, \tag{3.3}$$

where $\mathbf{D}_S$ is the constitutive matrix and $\boldsymbol{\varepsilon}_S$, which denotes the strains, relates to the displacements according to the kinematic relation

$$\boldsymbol{\varepsilon}_S = \tilde{\nabla}\mathbf{u}_S\,. \tag{3.4}$$

By multiplying Eq. (3.1) with an arbitrary weight function $\mathbf{v}_S$ and integrating over the structural domain which is represented by the volume V, the following expression is obtained

$$\int_{\Omega_S} \mathbf{v}_S^{\mathsf{T}} \left(\tilde{\nabla}^{\mathsf{T}}\sigma_S - \rho_S \frac{\partial^2 \mathbf{u}_S}{\partial t^2} + \mathbf{b}_S \right) dV = 0\,. \tag{3.5}$$

Applying Green-Gauss theorem on the first term in Eq. (3.5) while introducing a new quantity $\mathbf{t}_S$ which denotes the surface traction vector, yields the weak formulation

$$\int_{\Omega_S} \mathbf{v}_S^{\mathsf{T}}\, \rho_S \frac{\partial^2 \mathbf{u}_S}{\partial t^2}\, dV + \int_{\Omega_S} \left(\tilde{\nabla}\mathbf{v}_S\right)^{\mathsf{T}} \sigma_S\, dV - \int_{\partial\Omega_S} \mathbf{v}_S^{\mathsf{T}}\, \mathbf{t}_S\, dS - ... \tag{3.6}$$

$$\int_{\Omega_S} \mathbf{v}_S^{\mathsf{T}}\, \mathbf{b}_S\, dV = 0\,,$$

in which $\partial\,\Omega_S$ is the boundary of the structural domain and S is the surface of the volume V. Discretizing the continuum structure into finite sized elements while introducing the FE approximations following the Galerkin method

$$\mathbf{u}_S = \mathbf{N}_S\, \mathbf{a}_S\,, \tag{3.7}$$

$$\mathbf{v}_S = \mathbf{N}_S\, \mathbf{c}_S\,,$$

with $\mathbf{c}_S$ being an arbitrary matrix, $\mathbf{a}_S$ being the nodal displacement vector and $\mathbf{N}_S$ containing the FE interpolation functions – yields upon insertion into Eq. (3.6) the expression

$$\int_{\Omega_S} \mathbf{N}_S^\mathsf{T} \rho_S \mathbf{N}_S \, dV \, \ddot{\mathbf{a}}_S + \int_{\Omega_S} \left(\tilde{\nabla}\mathbf{N}_S\right)^\mathsf{T} \mathbf{D}_S \tilde{\nabla}\mathbf{N}_S \, dV \, \mathbf{a}_S = ... \tag{3.8}$$
$$\int_{\partial\Omega_S} \mathbf{N}_S^\mathsf{T} \mathbf{t}_S \, dS + \int_{\Omega_S} \mathbf{N}_S^\mathsf{T} \mathbf{b}_S \, dV \, ,$$

where use has been made of the relations (3.3) and (3.4). Now assigning the terms in Eq. (3.8) the following denotations

$$\mathbf{M}_S = \int_{\Omega_S} \mathbf{N}_S^\mathsf{T} \rho_S \mathbf{N}_S \, dV \; ; \quad \mathbf{K}_S = \int_{\Omega_S} \left(\tilde{\nabla}\mathbf{N}_S\right)^\mathsf{T} \mathbf{D}_S \tilde{\nabla}\mathbf{N}_S \, dV \; ; \tag{3.9}$$
$$\mathbf{f}_{b,S} = \int_{\partial\Omega_S} \mathbf{N}_S^\mathsf{T} \mathbf{t}_S \, dS \; ; \quad \mathbf{f}_{l,S} = \int_{\Omega_S} \mathbf{N}_S^\mathsf{T} \mathbf{b}_S \, dV \, ,$$

where $\mathbf{M}_S$ is the mass matrix, $\mathbf{K}_S$ the stiffness matrix, $\mathbf{f}_{b,S}$ the boundary load vector and $\mathbf{f}_{l,S}$ the body load vector – yields the expression

$$\mathbf{M}_S \, \ddot{\mathbf{a}}_S + \mathbf{K}_S \, \mathbf{a}_S = \mathbf{f}_{b,S} + \mathbf{f}_{l,S} \, , \tag{3.10}$$

which is the FE formulation of the equation of motion which governs the structural domain in a structure–acoustic system [9]. If damping is taken into account, then the term $\mathbf{C}_S \, \dot{\mathbf{a}}_S$ is added to the left-hand side of Eq. (3.10).

3.1.2 Acoustic Fluid Domain

An undamped acoustic fluid is governed by the nonhomogeneous wave equation under the assumption that the fluid is inviscid, irrotational and undergoes small translations. The governing wave equation for such a fluid leads as follows

$$\frac{\partial^2 p_F}{\partial t^2} - c_0^2 \nabla^2 p_F = 0 \, , \tag{3.11}$$

where p_F is the dynamic pressure, c_0 the speed of sound and ∇ is a gradient vector according to

$$\nabla = \left[\begin{array}{ccc} \dfrac{\partial}{\partial x} & \dfrac{\partial}{\partial y} & \dfrac{\partial}{\partial z} \end{array} \right]^\mathsf{T} . \tag{3.12}$$

Multiplying Eq. (3.11) by an arbitrary weight function v_F and integrating over the acoustic fluid domain which is represented by the volume V, yields

$$\int_{\Omega_F} v_F \left(\frac{\partial^2 p_F}{\partial t^2} - c_0^2 \nabla^2 p_F \right) dV = 0 \, , \tag{3.13}$$

which with the help of Green's theorem gives the weak formulation

$$\int_{\Omega_F} v_F \frac{\partial^2 p_F}{\partial t^2}\, dV + c_0^2 \int_{\Omega_F} \nabla v_F \nabla p_F \, dV = c_0^2 \int_{\partial\Omega_F} v_F \nabla p_F \, \mathbf{n}_F \, dS \,, \tag{3.14}$$

where $\partial\,\Omega_F$ is the boundary of the acoustic fluid domain and $\mathbf{n}_F$ is a normal vector acting on the boundary and pointing outwards from the domain. Inserting the FE approximations following the Galerkin method

$$\begin{aligned} p_F &= \mathbf{N}_F \, \mathbf{p}_F \,, \\ v_F &= \mathbf{N}_F \, \mathbf{c}_F \,, \end{aligned} \tag{3.15}$$

into the weak formulation (3.14), in which $\mathbf{c}_F$ is an arbitrary matrix, $\mathbf{p}_F$ is the nodal pressure vector and $\mathbf{N}_F$ is the FE interpolation function matrix, gives

$$\begin{aligned} &\int_{\Omega_F} \mathbf{N}_F^{\mathsf{T}} \, \mathbf{N}_F \, dV \, \ddot{\mathbf{p}}_F + c_0^2 \int_{\Omega_F} (\nabla \mathbf{N}_F)^{\mathsf{T}} \, \nabla \mathbf{N}_F \, dV \, \mathbf{p}_F = ... \\ &c_0^2 \int_{\partial\Omega_F} \mathbf{N}_F^{\mathsf{T}} \, \mathbf{n}_F \nabla p_F \, dS \,. \end{aligned} \tag{3.16}$$

Introducing the following denotations

$$\begin{aligned} &\mathbf{M}_F = \int_{\Omega_F} \mathbf{N}_F^{\mathsf{T}} \, \mathbf{N}_F \, dV \,; \quad \mathbf{K}_F = c_0^2 \int_{\Omega_F} (\nabla \mathbf{N}_F)^{\mathsf{T}} \, \nabla \mathbf{N}_F \, dV \,; \\ &\mathbf{f}_{b,F} = c_0^2 \int_{\partial\Omega_F} \mathbf{N}_F^{\mathsf{T}} \, \mathbf{n}_F \nabla p_F \, dS \,, \end{aligned} \tag{3.17}$$

yields upon insertion into Eq. (3.16), the FE formulation of the nonhomogeneous wave equation

$$\mathbf{M}_F \, \ddot{\mathbf{p}}_F + \mathbf{K}_F \, \mathbf{p}_F = \mathbf{f}_{b,F} \,, \tag{3.18}$$

where $\mathbf{M}_F$ is the mass matrix, $\mathbf{K}_F$ the stiffness matrix and $\mathbf{f}_{b,F}$ the boundary load vector [9]. The assumption of undamped fluid implies neglecting fluid viscosity, which is considered reasonable in low frequency ranges when studying wave propagation in slightly viscous fluids such as air. If one wants to consider fluid viscosity, which is essential when studying wave propagation through porous media [10], then the continuum formulation in Eq. (3.11) is modified according to

$$\frac{\partial^2 p_F}{\partial t^2} + \frac{R}{\rho_0} \frac{\partial p_F}{\partial t} - c_0^2 \nabla^2 p_F = 0 \,, \tag{3.19}$$

where R is the flow resistivity and ρ_0 is the static density. This gives the following FE formulation

$$\mathbf{M}_F \, \ddot{\mathbf{p}}_F + \mathbf{C}_F \, \dot{\mathbf{p}}_F + \mathbf{K}_F \, \mathbf{p}_F = \mathbf{f}_{b,F} \,, \tag{3.20}$$

which is the governing nonhomogeneous wave equation for damped fluid [11].

3.1.3 Coupling of Domains

Interaction of the structure domain and the acoustic fluid domain in a structure–acoustic system is ensured by defining coupling conditions at the interface of the domains. The coupling conditions take the form of continuous displacement and acoustic pressure according to

$$\mathbf{u}_S \mathbf{n}_F = \mathbf{u}_F \mathbf{n}_F \,, \tag{3.21}$$

$$\boldsymbol{\sigma}_S\big|_{\mathbf{n}_F} = -p_F \,,$$

in which the expression $\boldsymbol{\sigma}_S\big|_{\mathbf{n}_F}$ denotes the stress components parallel to the normal vector $\mathbf{n}_F$. Introducing the spatial coupling matrix

$$\mathbf{H}_{SF} = \int_{\partial\Omega_{SF}} \mathbf{N}_S^{\mathsf{T}}\, \mathbf{n}_F\, \mathbf{N}_F \, dS \,, \tag{3.22}$$

enables the boundary load vector of the structure domain, Eq. (3.9), and of the acoustic fluid domain, Eq. (3.17), to be expressed as

$$\mathbf{f}_{b,S} = \mathbf{H}_{SF}\, \mathbf{p}_F \,, \tag{3.23}$$

$$\mathbf{f}_{b,F} = -\rho_0\, c_0^2\, \mathbf{H}_{SF}^{\mathsf{T}}\, \ddot{\mathbf{a}}_S \,.$$

By considering the coupling conditions in Eq. (3.21), the governing equations of the separate domains can be combined to describe the coupled system [9]

$$\begin{bmatrix} \mathbf{M}_S & \mathbf{0} \\ \rho_0\, c_0^2\, \mathbf{H}_{SF}^{\mathsf{T}} & \mathbf{M}_F \end{bmatrix} \begin{bmatrix} \ddot{\mathbf{a}}_S \\ \ddot{\mathbf{p}}_F \end{bmatrix} + \begin{bmatrix} \mathbf{K}_S & -\mathbf{H}_{SF} \\ \mathbf{0} & \mathbf{K}_F \end{bmatrix} \begin{bmatrix} \mathbf{a}_S \\ \mathbf{p}_F \end{bmatrix} = ... \tag{3.24}$$

$$\begin{bmatrix} \mathbf{f}_{l,S} \\ \mathbf{0} \end{bmatrix} + \begin{bmatrix} \mathbf{f}_{b,S} \\ \mathbf{f}_{b,F} \end{bmatrix} .$$

If damped fluid is considered, refer back to Eq. (3.20), then the system is expanded to include

$$\begin{bmatrix} \mathbf{M}_S & \mathbf{0} \\ \rho_0\, c_0^2\, \mathbf{H}_{SF}^{\mathsf{T}} & \mathbf{M}_F \end{bmatrix} \begin{bmatrix} \ddot{\mathbf{a}}_S \\ \ddot{\mathbf{p}}_F \end{bmatrix} + \begin{bmatrix} \mathbf{C}_S & \mathbf{0} \\ R\, c_0^2\, \mathbf{H}_{SF}^{\mathsf{T}} & \mathbf{C}_F \end{bmatrix} \begin{bmatrix} \dot{\mathbf{a}}_S \\ \dot{\mathbf{p}}_F \end{bmatrix} + ... \tag{3.25}$$

$$\begin{bmatrix} \mathbf{K}_S & -\mathbf{H}_{SF} \\ \mathbf{0} & \mathbf{K}_F \end{bmatrix} \begin{bmatrix} \mathbf{a}_S \\ \mathbf{p}_F \end{bmatrix} = \begin{bmatrix} \mathbf{f}_{l,S} \\ \mathbf{0} \end{bmatrix} + \begin{bmatrix} \mathbf{f}_{b,S} \\ \mathbf{f}_{b,F} \end{bmatrix} ,$$

in which the boundary load vector of the acoustic fluid domain takes the form

$$\mathbf{f}_{b,F} = -\rho_0\, c_0^2\, \mathbf{H}_{SF}^{\mathsf{T}}\, \ddot{\mathbf{a}}_S - R\, c_0^2\, \mathbf{H}_{SF}^{\mathsf{T}}\, \dot{\mathbf{a}}_S \,, \tag{3.26}$$

when the spatial coupling matrix is introduced [11].

3.1.4 Biot's Theory

A porous medium consists of two phases, namely a structural phase consisting of solid material, and a fluid phase. When studying acoustic wave propagation that occurs within a porous medium, one may invoke Biot's Theory which describes acoustic propagation by regarding the structural and fluid partitions in a porous medium and the coupling inbetween. The so called $\mathbf{u}_s - p_f$ formulation is a FE formulation of the acoustic wave propagation, derived using Biot's Theory, that relates the structural displacements $\mathbf{u}_s$ to the acoustic pressure p_f within a porous medium. The $\mathbf{u}_s - p_f$ formulation yields

$$\begin{bmatrix} -\omega^2\mathbf{M}_{ss} + \mathbf{K}_{ss} & -\mathbf{C}_{sp} \\ -\omega^2\mathbf{C}_{sp}^T & -\omega^2\mathbf{M}_{pp} + \mathbf{K}_{pp} \end{bmatrix} \begin{bmatrix} \mathbf{a}_s \\ \mathbf{p}_f \end{bmatrix} = \begin{bmatrix} \mathbf{f}_{b,s} \\ \mathbf{f}_{b,p} \end{bmatrix}, \tag{3.27}$$

where the index s denotes a variable in the structural partition of the porous medium domain and the index p denotes a variable in the fluid partition of the porous medium domain. The matrix $\mathbf{C}_{sp}$ refers to the coupling matrix at the boundary of the pourous medium and the acoustic fluid, denoted Ω_{PF}, according to

$$\mathbf{C}_{sp} = \tilde{\gamma} \int_{\Omega_{PF}} \mathbf{N}_s^\intercal \, \nabla \mathbf{N}_p \, dV \,. \tag{3.28}$$

For explanations of the variables above, and for complete derivation of Biot's Theory and the $\mathbf{u}_s - p_f$ formulation, the reader is referred to [9].

3.2 Equivalent Radiated Power

In order to understand and anticipate how vibrations are translated into structure–borne noise, one may use the so called equivalent radiated power (ERP). The sound power is given by

$$P = \frac{1}{2} \int_A \mathrm{Re}\,(p \, v_n^*) \, dA \,, \tag{3.29}$$

where p is the acoustic pressure, v_n^* is the structural normal velocity at the surface of the vibrating structure and A is the surface area of the said structure. Since there is a velocity continuity at the interface between the structure and the air, i.e. $v_n = v_{air}$, one may replace the acoustic pressure p in Eq. (3.29) using the relation

$$v_n = \frac{p}{\rho_0 \, c} \,, \tag{3.30}$$

where ρ_0 is the air density and c is the speed of sound in air. The equivalent radiated power can then be written as

$$\mathrm{ERP} = \frac{1}{2} \rho_0 \, c \int_A |v_n(\omega)|^2 \, dA \,. \tag{3.31}$$

ERP is an indicator of the vibrations which may lead to structure–borne noise radiation. High ERP is necessary but not sufficient for having high noise radiation [12].

3.3 Noise Transfer Function

Noise transfer function (NTF) is a type of FRF that relates the acoustic response of an excited system to its sinusoidal input. For explanation of FRF, refer back to Section 2.5. The NTF can be seen as an indicator of structure–borne noise sensitivity and is described as the complex ratio of sound pressure to input force according to

$$H(\omega) = \frac{\mathbf{p}^*}{\mathbf{p_0}}\,, \tag{3.32}$$

where $\mathbf{p}^*$ denotes the complex amplitudes of sound pressure and $\mathbf{p_0}$ denotes the complex amplitudes of input force [13].

Chapter 4

Example Case of Floor Panel and Carpet

The following chapter shows an example case of a simplified floor panel–carpet setup which was modelled using the FE method, in which three modelling techniques were adopted for representing the carpet in the setup. In the first model, the carpet was defined as a non-structural mass (NSM) added onto the panel. Although one may argue this choice of modelling is flawed and introduces a rough simplification of the actual behaviour, it is often used to save computational time and has been shown to be sufficient for studying dynamic interaction in low frequencies [1]. This choice of modelling trim components is often adopted in product development. In the other two models, geometrical and structural aspects of the carpet were further defined, with the aim of capturing a more accurate vibrational and acoustical behaviour of the panel–carpet setup for higher frequencies. In one of the models, linear elastic (LE) material properties were given to the carpet, whereas in the other model, the foam in the carpet was assigned porous elastic material (PEM) properties. While giving the carpet LE properties may be suitable to increase the accuracy of the model, the use of PEM is thought to be a more realistic representation of the solid and fluid phases of the porous carpet. This chapter serves as a basis for the next two chapters in which the vibration response (Chapter 5) and the acoustic radiation (Chapter 6) of the example case are simulated and analyzed.

4.1 Software and Finite Element Solvers

The numerical FE models were constructed using the software ANSA [14]. ANSA is a CAE pre-processing tool developed by Beta CAE systems. The software is used in numerous industries such as automotive, aerospace and maritime. An FE solver is needed in order to solve different types of FE problems. In this dissertation, MSC Nastran v.2021.0 [15] was used. The FE software Nastran was originally used by NASA. In 1965, the MSC corporation was awarded a contract to commercialize the software, which later became known as MSC Nastran [16]. MSC Nastran uses text files as input, where the FE model, as well as other parameters such as boundary and loading conditions, are defined. A specific solver needs to be chosen depending on the problem to be solved. Table 4.1 shows the MSC Nastran solvers used in this dissertation.

Solver	Solution sequence
103	Normal Modes
108	Direct Frequency Response
111	Modal Frequency Response

Table 4.1: MSC Nastran solvers used in this dissertation.

The output from MSC Nastran can be requested in the input file depending on the post-processor used. The post-processor used in this dissertation is META [17] which similarly to ANSA, is developed by Beta CAE systems. In order to visualize and present the output data, the program MATLAB [18] developed by MathWorks was utilized.

4.2 Geometry and Materials

Figure 4.1 shows the body structure of a vehicle produced by Volvo Cars, whose panel–carpet setup is the basis for the developed FE models. The floor carpet marked in yellow refers to the structure part whose vibro–acoustic interaction is of interest for this dissertation.

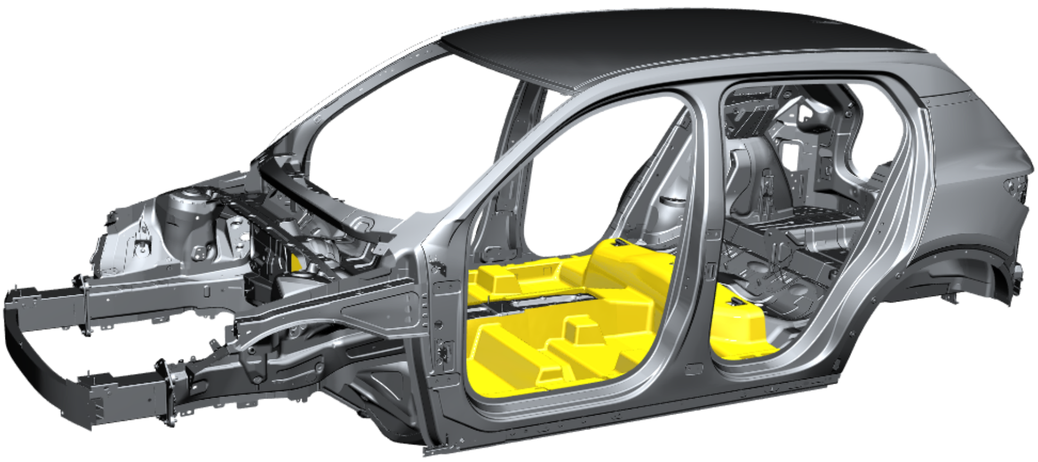

Figure 4.1: Body structure of a vehicle produced by Volvo Cars. Floor carpet shown in yellow. Credits: Volvo Cars.

For simplicity, a flat panel and carpet setup was assumed. The flat setup has the dimensions $400 \cdot 400$ mm^2 and is composed of a sheet metal panel on top of which an interior carpet is loosely applied without any adhesives. The panel has a thickness of 0.6 mm and is made of steel, whereas the carpet consists of two layers; a 23 mm thick foam layer and a 2 mm thick layer made of rubber material, so called heavy layer (HL). The HL is assumed to be fully glued onto the foam layer. Figure 4.2 shows the studied panel–carpet setup.

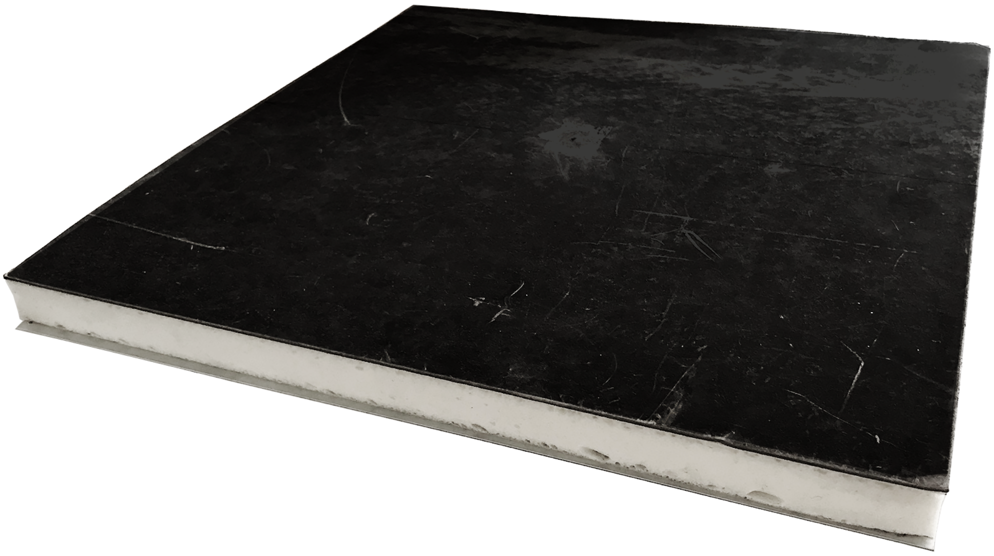

Figure 4.2: Studied floor panel and interior carpet setup, provided by Volvo Cars. The interior carpet is composed of a HL (black in the figure) glued on top of a foam layer (white). The interior carpet is resting upon the floor panel (grey).

The material properties that were used for each of the layers are presented in Table 4.2. When treating the foam material as a porous medium, then properties according to Table 4.3 were used instead. The material parameters were provided by Volvo Cars and their suppliers, with an exception for the damping value of the panel which was estimated based on what is deemed reasonable for steel. Some material parameters were chosen not to be disclosed, why a parameter range is listed instead. Units are given in N, mm, s and tonne.

Layer	E-modulus [N/mm^2]	Poisson's ratio [-]	Density [tonne/mm^3]	Damping ratio [-]
Panel	210000	0.3	7.85e-9	0.01
HL	80 – 200	0.2 – 0.4	1.1e-9 – 2.8e-9	0.02 – 0.08
Foam	0.08 – 0.20	0.2 – 0.4	4.5e-11 – 7.6e-11	0.10 – 0.20

Table 4.2: Material parameters when assuming linear elasticity.

Solid phase	E-modulus	0.08 – 0.20	[N/mm^2]
	Poisson's ratio	0.20 – 0.40	[-]
	Density	1.0e-9 – 2.0e-9	[tonne/mm^3]
	Damping ratio	0.10 – 0.20	[-]
Fluid phase	Fluid mass density	1.225e-12	[tonne/mm^3]
	Fluid speed of sound	343000	[mm/s]
	Fluid loss factor	0.01	[-]
Biot parameters	Biot factor	1.0	[-]
	Fluid viscosity	1.82e-11	[Ns/mm^2]
	Fluid Prandtl number	1.402	[-]
	Fluid gamma ratio	0.71	[-]
	Porosity	0.86 – 0.98	[-]
	Tortuosity	1.68 – 3.21	[-]
	Air flow resistivity	3.48e-8	[Ns/mm^4]
	Viscous characteristic length	0.010 – 0.045	[mm]
	Thermal characteristic length	0.230 – 0.380	[mm]

Table 4.3: Material parameters when assuming poro-elasticity for the foam.

4.3 Dynamic Excitation and Boundary Conditions

To simulate the vibro–acoustic response of the system, the floor panel was excited with a dynamic unit point load in the transverse z direction, subjecting the panel to a steady-state frequency sweep ranging from 0 to 1000 Hz. In order to excite a large number of vibration modes, the dynamic unit load was applied on an off-centre node with the coordinates (120, 160, 0) mm on the panel, see Figure 4.3.

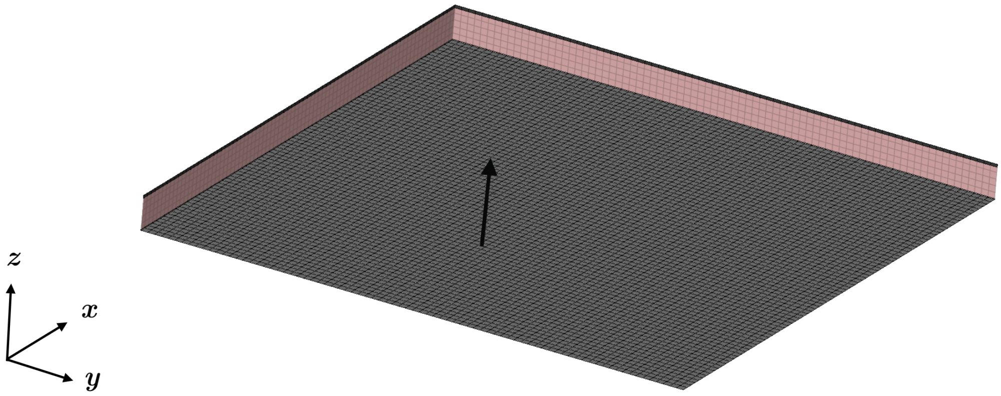

Figure 4.3: Placement of the dynamic unit load.

To reduce the effect of external factors that may influence the response of the system, and to easier reproduce the setup experimentally, free–free conditions were assumed. Free–free conditions imply that the model is suspended in a way allowing it to translate and rotate freely, and that no external constraints in the form of displacement boundary conditions are defined in the FE model.

4.4 Finite Element Modelling of Panel and Carpet

Numerical FE models were constructed using the software ANSA, in which three different modelling techniques were adopted for the carpet in the setup. Oftentimes, trim components such as carpets are either defined as a uniformly distributed mass or completely neglected when modelling a whole vehicle body in order to save computational time. In this dissertation, three modelling choices were explored in which the carpet was modelled as a:

- Uniformly distributed non-structural mass
- Continuous solid media with linear elastic properties
- Porous media with porous elastic properties

In all three models, the floor panel was treated the same, see Figure 4.4. The floor panel was modelled as a shell due to its slenderness, and was assigned material properties according to Table 4.2. The panel was further meshed with $5 \cdot 5$ mm^2 CQUAD4 elements according to the standard meshing criteria set by Volvo Cars.

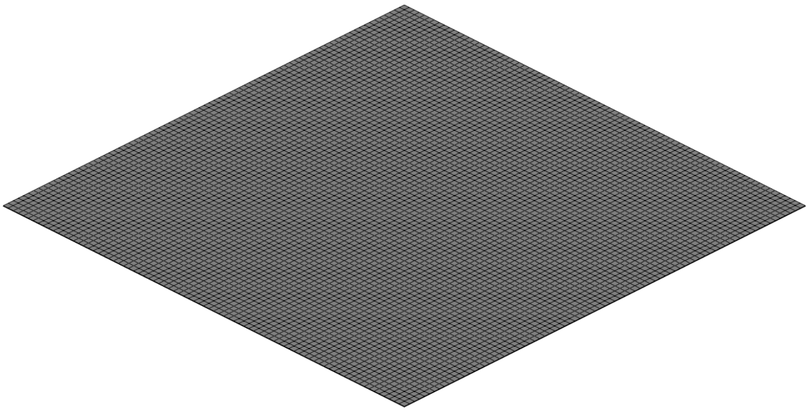

Figure 4.4: FE mesh used for the floor panel.

The mesh size was confirmed to yield seven elements per wavelength at the upper end of the studied frequency range, which fulfills the rule of thumb of having at least six nodes per wavelength; details can be found in Section 5.3.2.

4.4.1 Non-Structural Mass Model

In the first developed FE model, the carpet was modelled as a NSM. This was performed by defining the total mass of the carpet and applying it on the panel using NSML in MSC Nastran. The NSML command takes the assigned lumped mass value and distributes it evenly over the selected elements – here, the whole panel. To account for the damping effect the carpet provides, structural damping of the panel was modified to 3%. This value was chosen so that similar low–frequency resonance peaks were obtained when comparing to the LE and PEM models, see results in Section 5.1. This model is hereinafter referred to as the NSM model.

4.4.2 Linear Elastic Material Model

What the NSM approach fails to address is the fact that the carpet has mechanical and structural properties that result in internal dynamic and acoustic effects. Thus, a more accurate approach than to only consider the weight of the carpet would be to define its geometry and assign each layer its corresponding structural properties. The accuracy of this approach, however, comes on the behalf of increased computational time due to the increase in DoFs. In the second FE model, the geometry of the carpet was modelled and assigned isotropic linear elastic material properties according to Table 4.2. Since the HL is rather thin, it was modelled as a shell with a thickness of 2 mm. The HL was meshed with $5 \cdot 5$ mm^2 CQUAD4 elements similarly to the panel. The foam layer was then created by extruding the HL mesh downwards, resulting in CHEXA elements with the dimensions $5 \cdot 5 \cdot 4.6$ mm^3, see Figure 4.5. A glued connection between the HL and the foam was simulated by sharing common nodes at the interface. As the carpet is laid on top of the panel and is allowed to slide off, the bottom side of the foam was connected to the panel using RBE3 rigid elements restraining movement only in the vertical z axis. An RBE3 rigid element has one dependant node and several independent nodes. The dependant node is constrained to the average displacement of the independent nodes. This model is hereinafter referred to as the LE model.

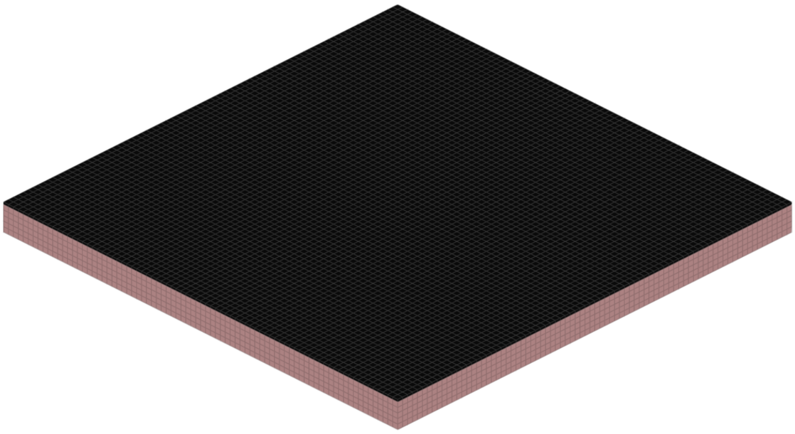

Figure 4.5: FE mesh used for the floor carpet.

4.4.3 Porous Elastic Material Model

A relatively new feature that has been implemented in the MSC Nastran environment is the ability to model porous elastic material (PEM) that is based on Biot's theory. The use of PEM is thought to give trim components a more realistic representation as it takes into account the internal acoustic pressure in air-filled cavities of the foam, and its interaction with the solid phase of the foam. The third FE model was modelled according to the PEM approach, in which the foam along with the HL, i.e. whole carpet, were defined as a TRMC unit in MSC Nastran. Similarly to the LE model, the foam layer was created with CHEXA elements with the dimensions $5 \cdot 5 \cdot 4.6$ mm^3 and was assigned porous elastic properties according to Table 4.3. The HL was then created by extruding the top layer of the foam upwards, resulting in one layer of CHEXA elements with the dimensions $5 \cdot 5 \cdot 2$ mm^3. The properties of the HL elements were modified to simulate solid shell elements, which are hybrid 3D elements specifically developed for transverse trim components made of isotropic solid material. Similarly to the LE model, a glued connection between the HL and the foam was simulated. The interface of the carpet and the panel was further coupled using the connection SSLIDE, which is thought to correspond to the RBE3 connection used in the LE model in which only z movement is restrained. This model is hereinafter referred to as the PEM model.

4.5 Implementation of External Acoustic Domain

An acoustic domain representing the surrounding air was implemented in order to enable prediction of sound radiation from the panel–carpet setup, see Figure 4.6. The acoustic domain was modelled using the shape of a sphere with a radius of 1800 mm, and was placed at the centre of gravity of each model.

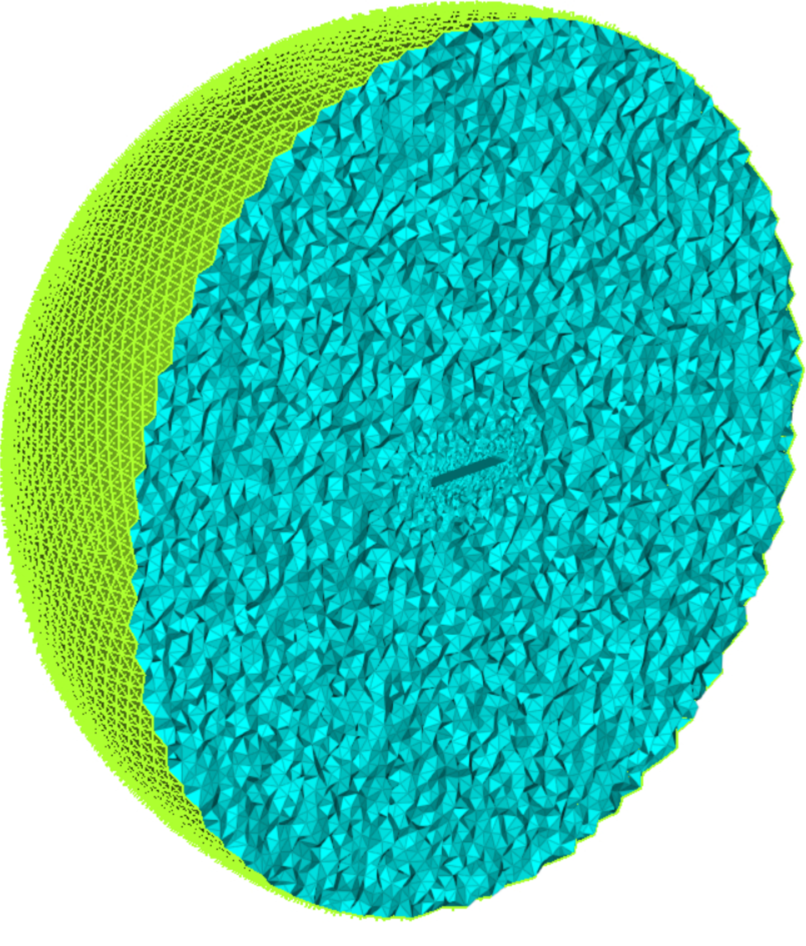

Figure 4.6: FE mesh of the external acoustic domain.

The acoustic analysis was limited to a frequency range of 100 – 600 Hz. The size of the sphere was chosen with respect to the largest wavelength passing through the acoustic domain, which occurs at the lower end of the frequency range of the analysis, see Table 4.4.

Frequency [Hz]	Wavelength [mm]
100	3440
600	573

Table 4.4: Acoustic wavelength in relation to frequency.

In order to generate fluid elements, a wrapped mesh surrounding the panel–carpet model was created. Both the wrapped surface and the outer shell of the sphere were meshed using CTRIA3 elements with an element length of 5 mm and 80 mm, respectively. The fluid was then generated by meshing the volume between the wrap and the outer shell of the sphere with solid elements of the type Tetra rapid. The elements were restricted to not violate the length 80 mm, in order to achieve at least six nodes per wavelength with respect to the shortest wavelength passing through the cavity, refer back to Table 4.4. Several microphones were placed on a vertical distance above the centre of gravity of panel–carpet model. To simulate free field conditions, CACINF elements representing infinite boundary were placed on the outer shell of the acoustic domain. The fluid was assigned material properties according to Table 4.5.

Fluid	Mass density [tonne/mm^3]	Speed of sound [mm/s]
Air	1.225e-12	343000

Table 4.5: Material parameters of the acoustic fluid.

Chapter 5

Simulation of Vibration Response

In this chapter, the vibration response of the NSM, LE and PEM models of the carpet described in Chapter 4, is presented and visualized in the form of ERP curves. In order to increase the credibility and reliability of the analyses conducted, convergence studies were performed to motivate FE settings such as mesh size and choice of FE solver. Since the PEM approach involves a number of input parameters, e.g. as seen in Table 4.3, sensitivity analyses concerning uncertain material and geometrical parameters were conducted in order to investigate the effects these uncertainties have on the vibration response. Consequently, knowledge regarding the sensitivity of the PEM approach may be established. In the figures of this chapter, black is generally used to visualize the panel response, whereas red is generally used to visualize the HL response. The HL response is thought to be representative of the carpet behaviour. In the said convergence studies and sensitivity analyses, the tag "(ref)" in legend is used to denote the reference model described in Chapter 4.

5.1 Vibration Response

Figure 5.1 shows the ERP for the three different models of the carpet using modal frequency response analysis in MSC Nastran. The ERP for the NSM model follows the LE and PEM models well up to about 120 Hz, implying that the carpet behaves as an added mass onto the panel in low frequency ranges. For frequencies higher than 120 Hz, clear deviation of the panel behaviour can be observed in the NSM model when compared to that of the LE and PEM models, which follow each other quite well throughout the studied frequency range. The fact that the LE and PEM models show very similar behaviour to each other confirms the assumption that the use of the coupling condition SSLIDE in the PEM approach corresponds to an RBE3 connection in the LE approach in which only the vertical z movement is restrained.

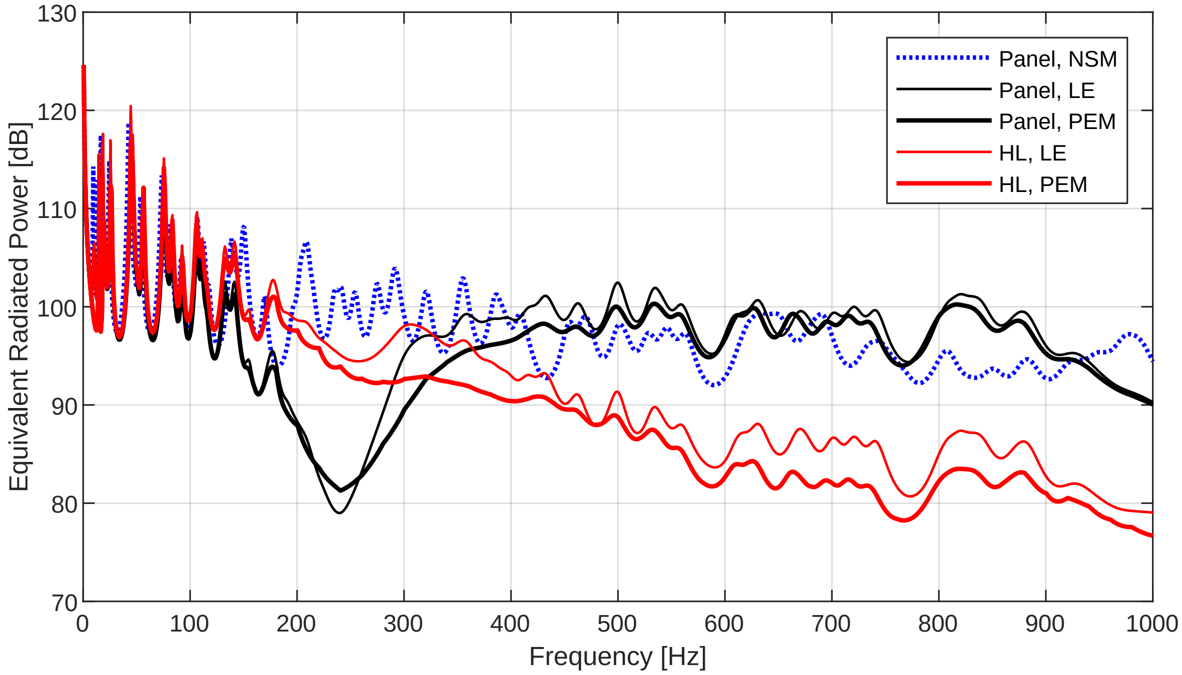

Figure 5.1: Vibration response of the panel–carpet setup due to a dynamic unit load using three different modelling techniques for the carpet. ERP shown for the panel and the carpet.

When analysing the LE and PEM models in Figure 5.1, a very distinct behaviour of the carpet – that the NSM model fails to demonstrate – can be observed in the vibration response throughout the studied frequency range. This behaviour can be characterized based on three regions, see Figure 5.2:

- Frequency range 0 – 120 Hz: The ERP curve of the panel coincides with that of the carpet, implying that the panel and the carpet vibrate in a uniform manner, radiating similar ERP levels. As the NSM model is able to capture this behaviour with sufficient accuracy, this may be interpreted as if the carpet in the setup purely behaves as a mass in this region. Therefore, it may be concluded that there is no need for complicated modelling choices when studying vibration response in low frequency ranges.
- Frequency range 120 – 430 Hz: The co-swinging of the panel and the carpet is disrupted as the ERP curves branch out. The vibration of the floor panel declines remarkably and reaches its lowest point, whereas the carpet stays at resonance. The NSM model fails to replicate this behaviour, leading to inaccurate results. For frequencies within this range, it is therefore not recommended to use the NSM approach – modelling choices with higher accuracy, such as LE or PEM, are needed.
- Frequency range 430 – 1000 Hz: After reaching its lowest point, the panel vibration increases significantly, whereas the carpet vibration drops gradually throughout this range. Due to the significant amplitude difference between the vibration of the panel and the carpet, the carpet can be seen as vibration-isolated in higher frequency ranges. An interesting observation is that the NSM model after around 450 Hz is somewhat able to capture parts of the panel response. This

is most likely due to the fact that the carpet in this range is vibration-isolated and behaves as an added mass with very low dynamic contribution.

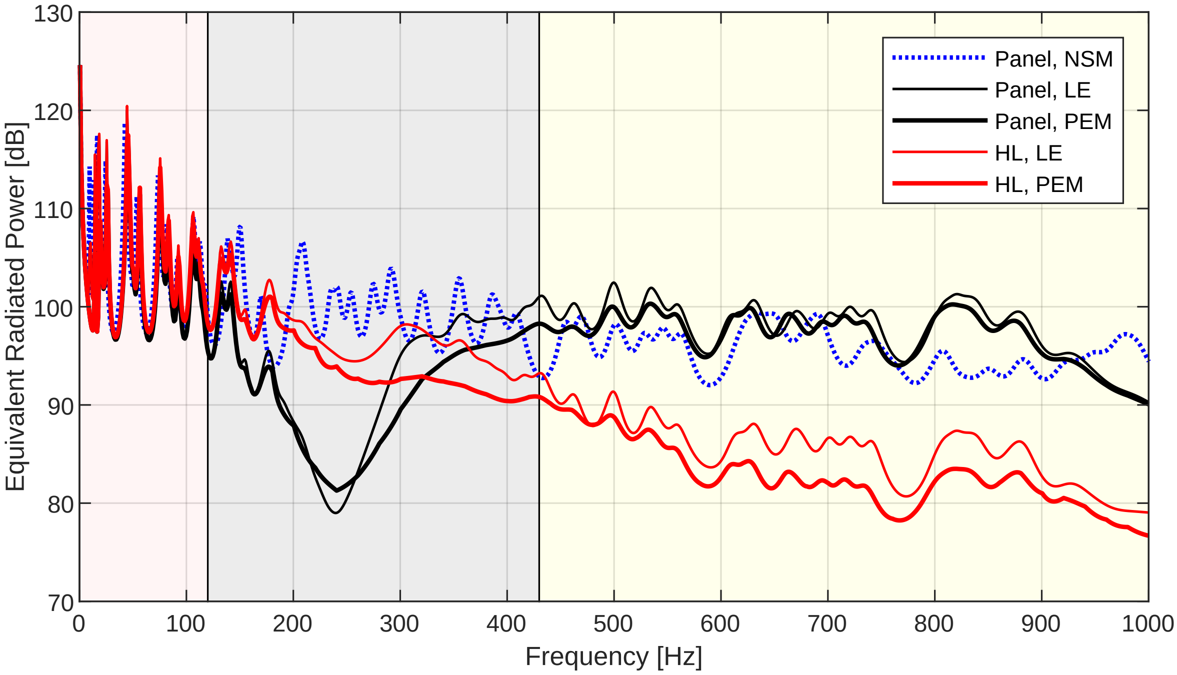

Figure 5.2: Three frequency regions with characteristic vibration behaviour.

5.2 Operating Deflection Shape

The operating deflection shape (ODS) is a type of analysis that animates the vibration response of a structure when subjected to a dynamic load. The ODS for the panel–carpet setup was computed for various frequencies in order to visualize the vibrational pattern and amplitude of the panel and HL. The frequencies at which ODS was computed are 118 Hz, 238 Hz, 325 Hz and 542 Hz, which are frequencies from each of the regions shown in Figure 5.2. The results are shown in Figure 5.3 in the form of 3D still view. As can be seen in Figure 5.3 (a), the ODS suggests that at frequency 118 Hz, the panel and the HL vibrate in the same direction and are of similar amplitude. This behaviour can be observed throughout the first region of Figure 5.2 and is therefore assumed to be representative of the vibrational behaviour at low frequencies. Two frequencies were examined in the second region of Figure 5.2, 238 Hz where the panel hits its lowest ERP level whilst the carpet is resonating, and 325 Hz where the ERP curves of the panel and HL intersect. Figure 5.3 (b) suggests that the amplitude of the vibrations in the HL is much greater than that of the panel, whereas Figure 5.3 (c) shows a much more complex behaviour in which the panel and the HL vibrate in different directions with similar amplitude. In the third region of Figure 5.2, frequency 542 Hz was examined for which Figure 5.3 (d) implies that the panel demonstrates much larger vibrations in relation to the carpet whose response is negligible.

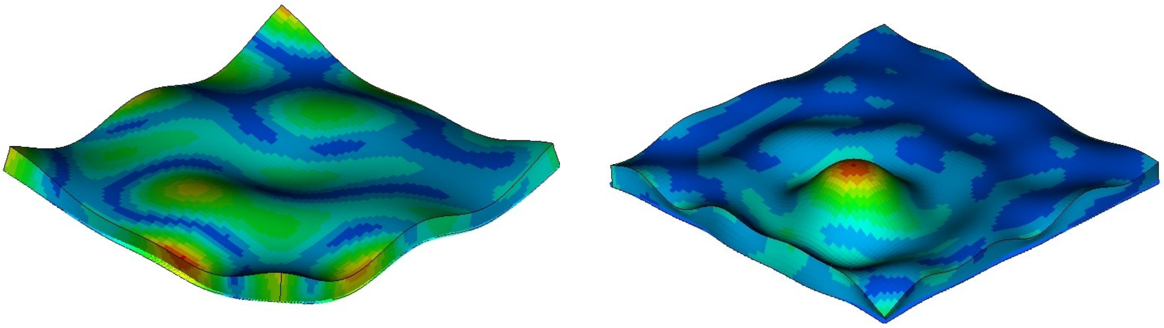

(a) Frequency 118 Hz. (b) Frequency 238 Hz.

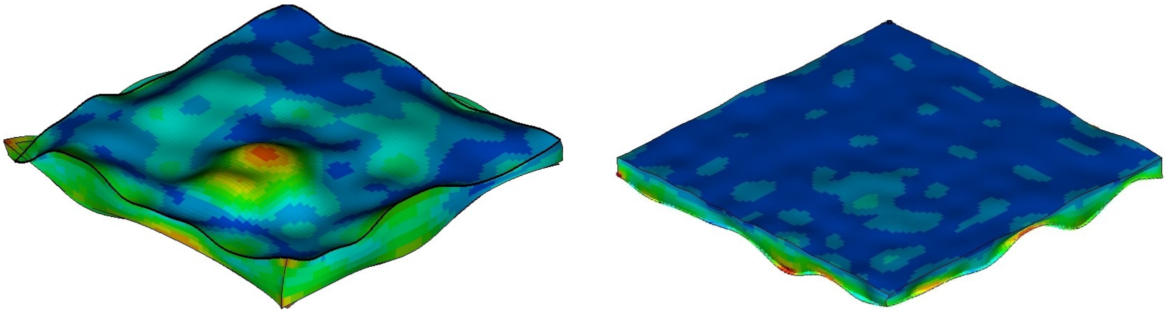

(c) Frequency 325 Hz. (d) Frequency 542 Hz.

Figure 5.3: ODS at four different frequencies to visualize characteristic vibration response of the panel–carpet setup.

In conclusion, ODS confirms what intuitively seems to be the case when interpreting the ERP curves. As the direction of the vibrations is harder to interpret in still view, the ODS was modified in order to illustrate the trend of the vibrations of the panel and HL, respectively – see Figure 5.4 which shows the panel and HL seen from above. Two colors were used to mark the two vibration directions, up and down, so that when overlapped, it becomes clear if the panel and HL resonate in a uniform or a counteracting manner.

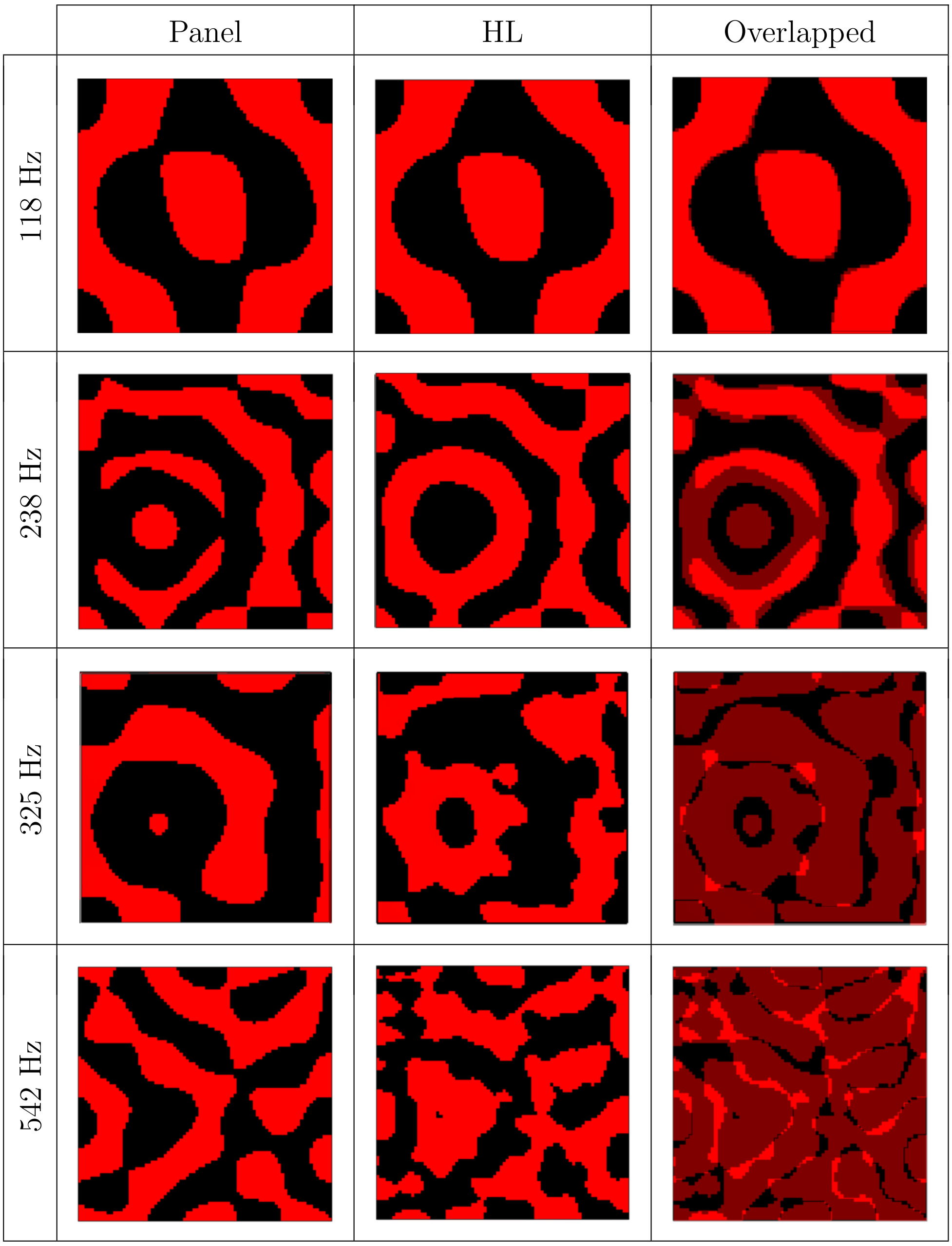
Panel
HL
Overlapped
118 Hz
238 Hz
325 Hz
542 Hz

Figure 5.4: Panel and HL seen from above. ODS modified to illustrate vibration trends in the panel and the HL at the different frequencies. Red and black used to represent opposite vibration directions. If dark red is obtained when overlapped, the components vibrate in counteracting manner. This figure gives no information regarding the amplitude.

5.3 Convergence Studies for Finite Element Settings

To increase the reliability and confirm the numerical accuracy of the results presented in this dissertation, convergence studies were performed and are presented in this section. The purpose of the convergence studies is to motivate and give credibility to the FE settings used in the analyses. The convergence studies were limited to the PEM model with an exception for the first study presented which concerns the use of the FE solver.

5.3.1 Direct and Modal Analysis

When computing the frequency response of a system, two approaches through which one may conduct the analysis are available – direct frequency response analysis (SOL108 in MSC Nastran) and modal frequency response analysis (SOL111). The analyses performed in this dissertation were conducted using SOL111, in which modes up to 1200 Hz for the structure, and up to 2000 Hz for the fluid when applicable, were computed. Although there exist guidelines that help determine whether SOL108 or SOL111 is most suitable for the problem at hand, the reason for choosing SOL111 is that the PEM approach is not fully supported to be computed through SOL108 in MSC Nastran. Furthermore, using SOL111 saves computational time as it excludes higher-order modes and reduces the studied system. Therefore, to eliminate any possible differences or errors due to the use of different FE solvers for the different models, it was concluded to apply SOL111 for all analyses performed in this dissertation. Figure 5.5 compares modal and direct frequency response for the NSM and LE models, respectively.

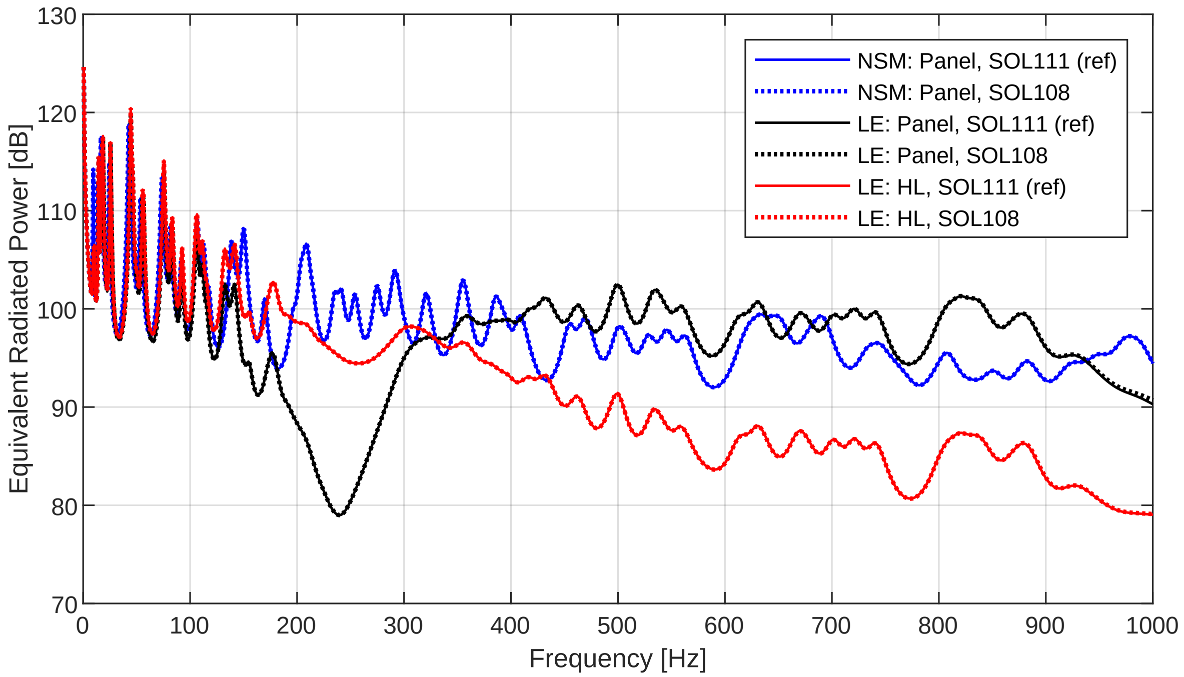

Figure 5.5: ERP response when using modal frequency response analysis (SOL111) and direct frequency response analysis (SOL108).

As could be seen in Figure 5.5, no visible difference can be distinguished when using the two solvers – implying that the use of SOL111 is reliable for the studied frequency range. Furthermore, the results affirm that eliminating modes higher than 1200 Hz for the structure in the system does not interfere with the accuracy of the results.

5.3.2 Mesh Criteria

The numerical accuracy highly depends on the mesh size of the model. Furthermore, the smaller the mesh size, the larger the computational time, and vice versa. As mentioned previously, refer back to Section 4.4, a common rule of thumb is to have at least six nodes per wavelength. By following this rule of thumb, one will retrieve enough data points per wavelength to accurately represent the requested output data. In order to validate and give credibility to the mesh size used in this dissertation, a study concerning mesh size was carried out, where the mesh size was increased to 8 mm and decreased to 3 mm. Figure 5.6 shows the obtained results.

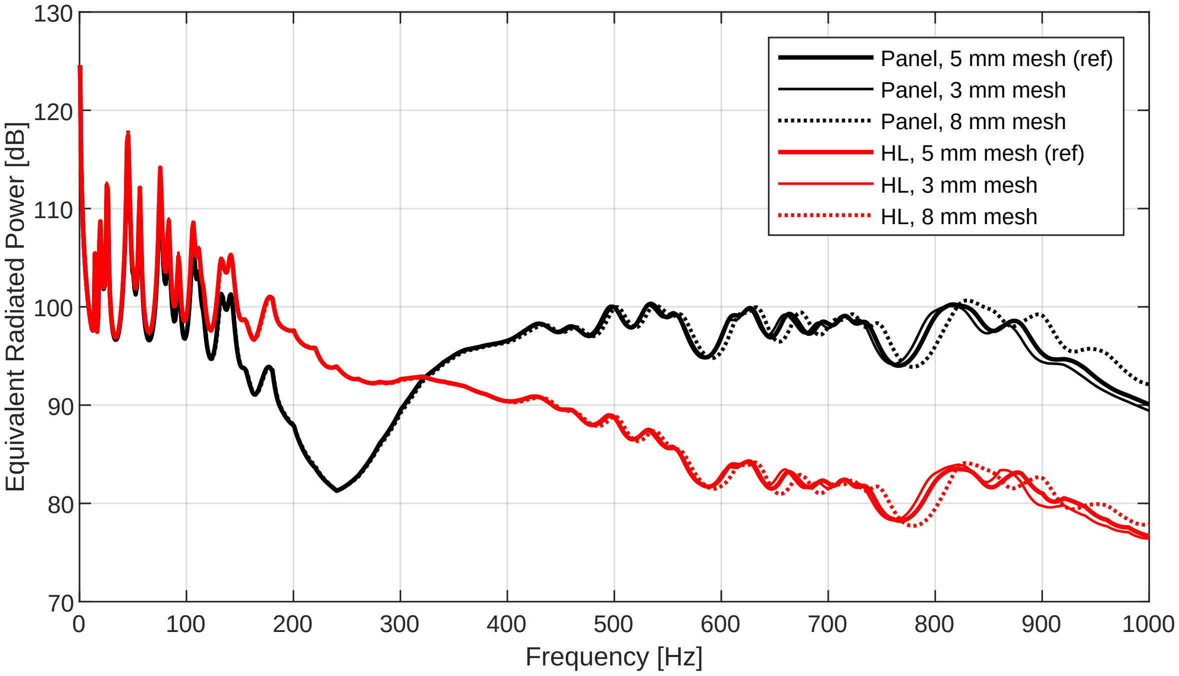

Figure 5.6: ERP response when the mesh size was increased to 8 mm and decreased to 3 mm, in relation to the original size of 5 mm.

As can be seen in Figure 5.6, there is virtually no difference in ERP up to around 600 Hz when comparing mesh sizes. This marginal difference continues up to 1000 Hz for the model with 3 mm mesh. Between 600 and 1000 Hz, when the model was meshed with 8 mm mesh, the data points retrieved start to deviate from the reference model more. This behaviour is however expected, since the wavelength becomes smaller with increased frequency. It is therefore concluded that the mesh size used in this dissertation is able to fully represent the requested data with sufficient accuracy.

5.4 Sensitivity Studies for Porous Elastic Material Model

A number of sensitivity studies regarding uncertain parameters were conducted on the PEM model. The purpose of the studies is to investigate the sensitivity of the studied setup and the PEM approach, as well as determine the parameters that have the most significant influence on the vibration response of the setup.

5.4.1 Panel–Carpet Coupling

The coupling conditions of the interface between the panel and the carpet were investigated. Two possible coupling conditions in MSC Nastran, applicable for the studied setup, were considered; SSLIDE in which the carpet is allowed to slide off the panel, and SGLUED in which the carpet is assumed to be fully glued onto the panel. Figure 5.7 shows the obtained results.

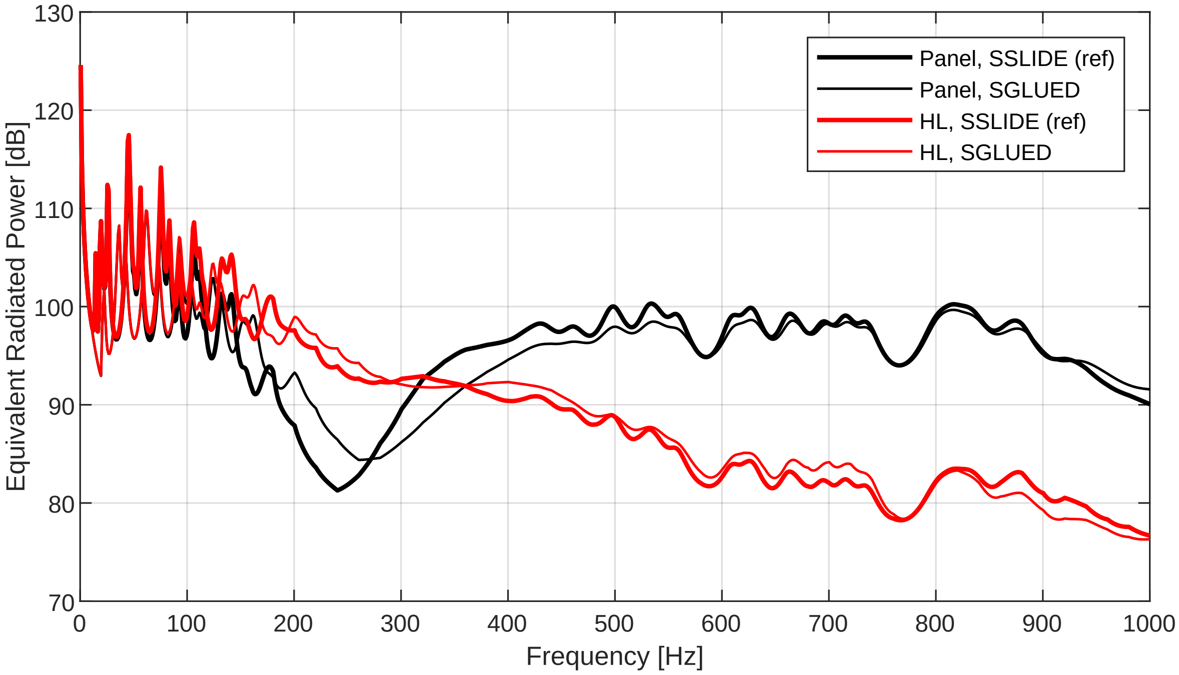

Figure 5.7: ERP response when the connection between panel and carpet was set to SSLIDE and SGLUED, respectively.

As Figure 5.7 suggests, the most significant difference in vibration response can be observed within the frequency range 0 – 500 Hz. At low frequencies where the panel and the carpet vibrate in a uniform manner – first region in Figure 5.2 – the glued setup radiate lower ERP levels which implies that the vibrations are slightly damped in comparison to the setup in which no adhesive is used between the panel and the carpet. Furthermore, it can be observed that the dip of the panel vibration at about 240 Hz and the intersection of the ERP curves for the panel and HL at about 320 Hz, are shifted towards higher frequencies, which most likely stems from the fact that using adhesives contributes to an increased stiffness in the setup.

5.4.2 Panel Thickness

The floor panel in the studied panel–carpet setup is 0.6 mm in thickness. Manufacturers, however, have a certain geometric tolerance in production. It is therefore of interest to study variations of the panel thickness according to the manufacturing tolerance and investigate its effects on the vibration response of the setup. Figure 5.8 shows the results when the tolerance was varied by ± 0.05 mm.

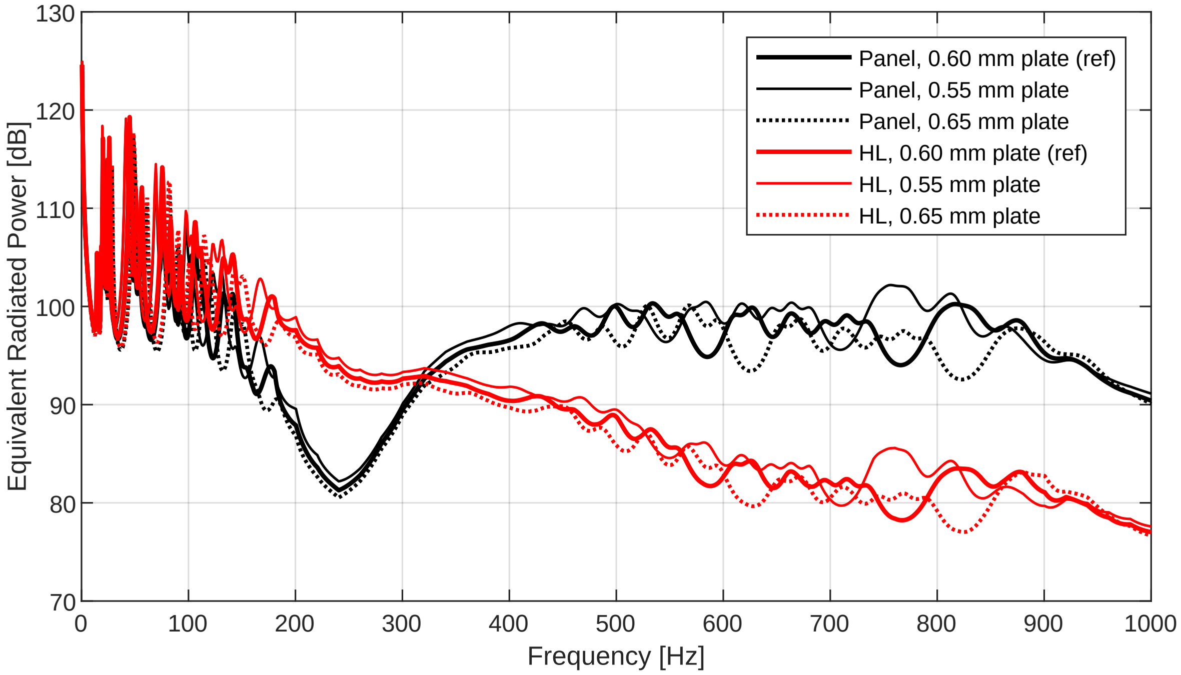

Figure 5.8: ERP response when the manufacturing tolerance of the panel thickness was varied by ± 0.05 mm.

As seen in Figure 5.8, there is a small divergence from the reference model up to about 450 Hz. Looking at the higher frequencies, 450 Hz and beyond, a complete shift in resonance peaks can be observed when comparing to the reference model. This is due to the fact that a change as small as ± 0.05 mm in thickness not only changes the geometry of the panel, but also its stiffness and mass. This change in stiffness and mass properties may lead to different resonance behaviour that is more pronounced at higher frequencies.

5.4.3 Material Damping

The damping values that were used for the different materials in the panel–carpet setup were provided by Volvo Cars, refer back to Section 4.2. The damping values for the foam and HL are based on measurements and laboratory testing by the supplier, and all such measured values come with uncertainties. The damping values were modified by reasonable factors for each of the material types, to minimize any possible errors with respect to the measurements and to check the sensitivity of the vibration response. The results are shown in Figure 5.9 to 5.11.

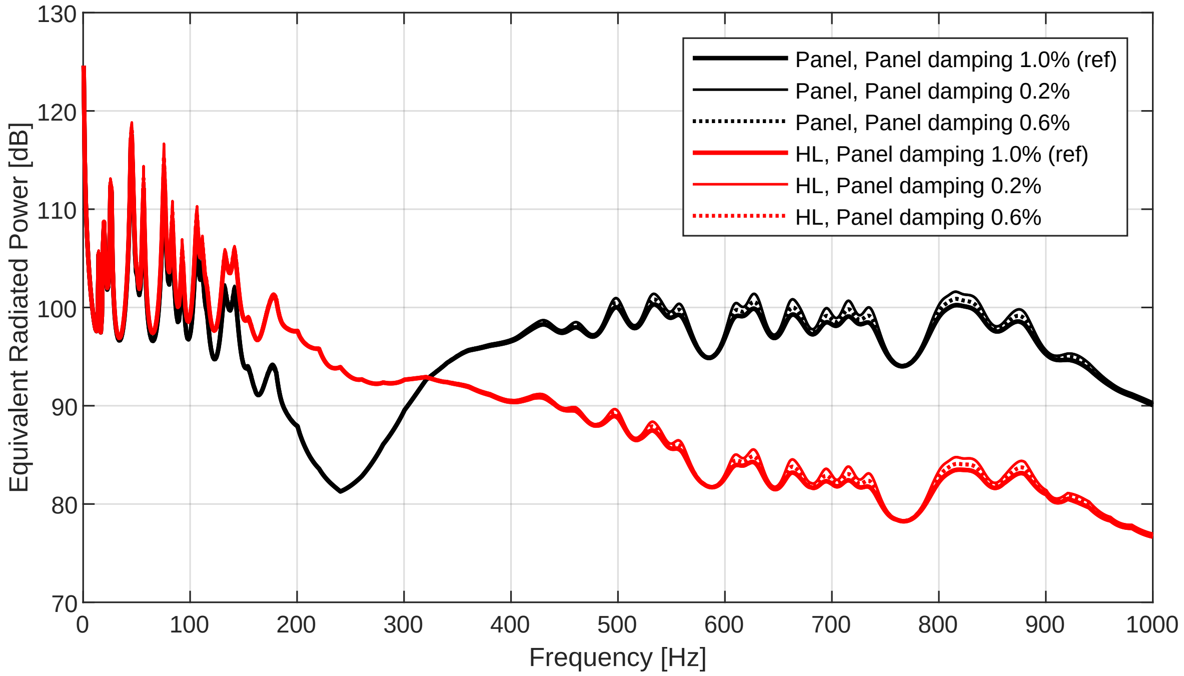

Figure 5.9: ERP response when the damping of the steel panel was set to 0.2% and 0.6% respectivly.

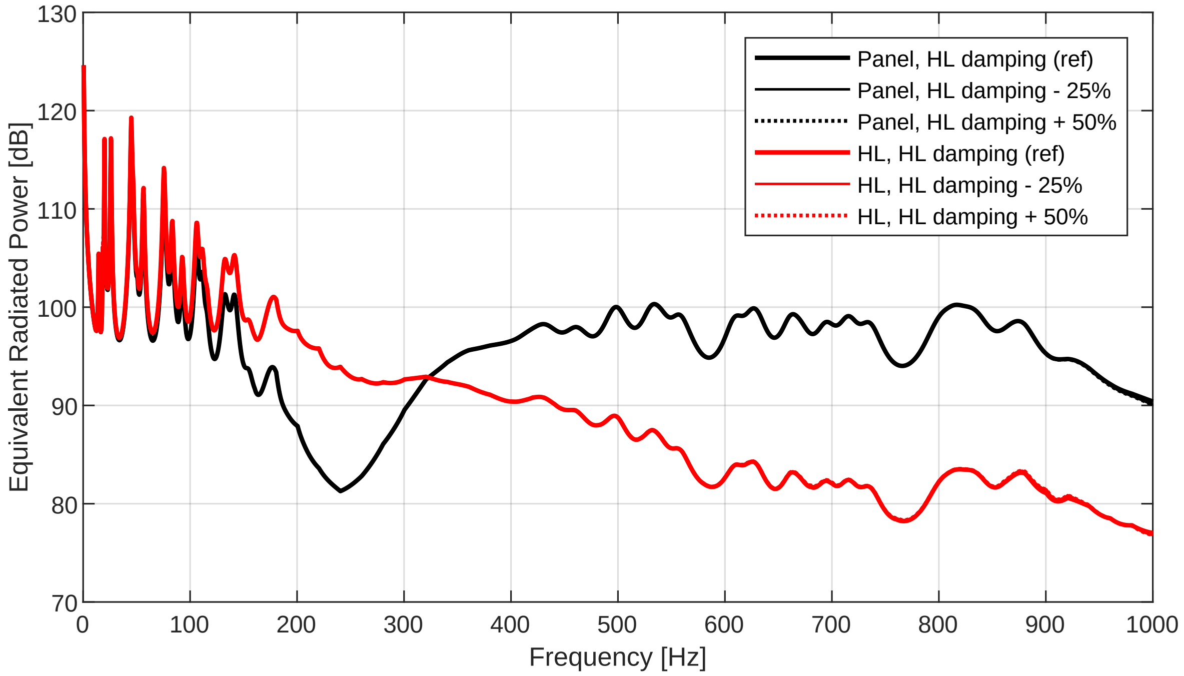

Figure 5.10: ERP response when the damping value of the HL was varied by -25% and +50% relative to the reference value.

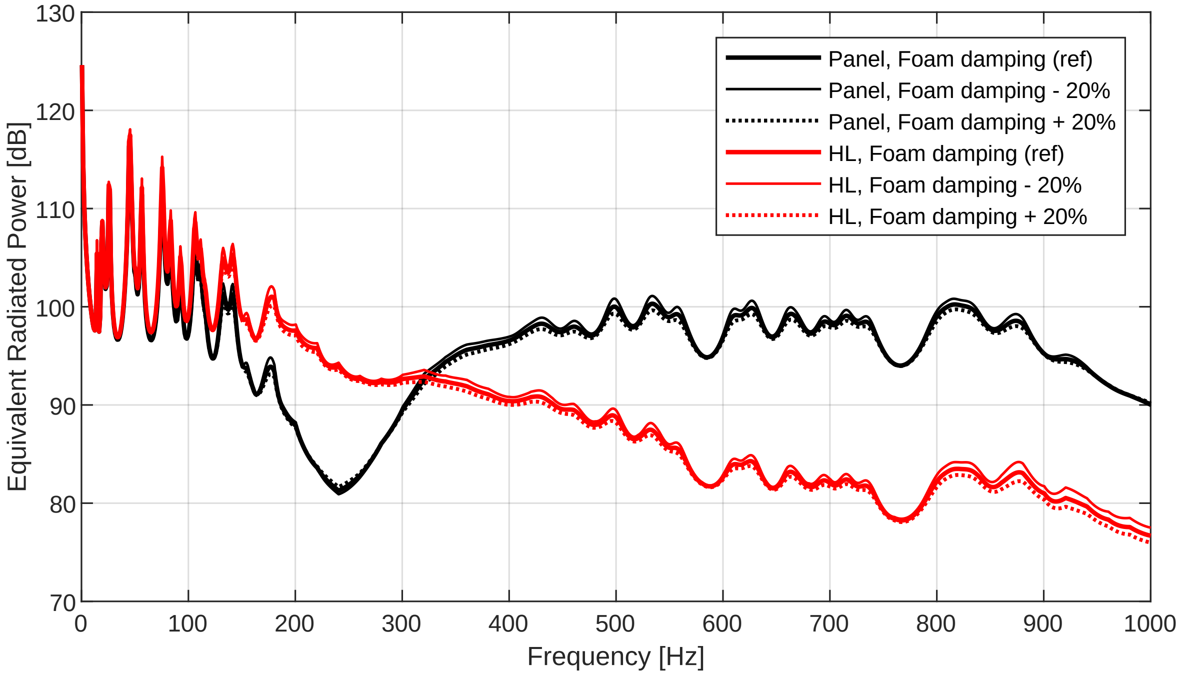

Figure 5.11: ERP response when the damping value of the foam was varied by ±20% relative to the reference value.

It is apparent from the results shown in Figure 5.9 to 5.11 that there was little deviation from the reference model. Damping of composite structures is a complex phenomenon which does not solely depend on the material damping parameters, but also on the interaction between the composite layers, where friction may occur.

5.4.4 Young's modulus of Heavy Layer

The Young's modulus of the HL was varied with ±10 MPa. The results are shown in Figure 5.12.

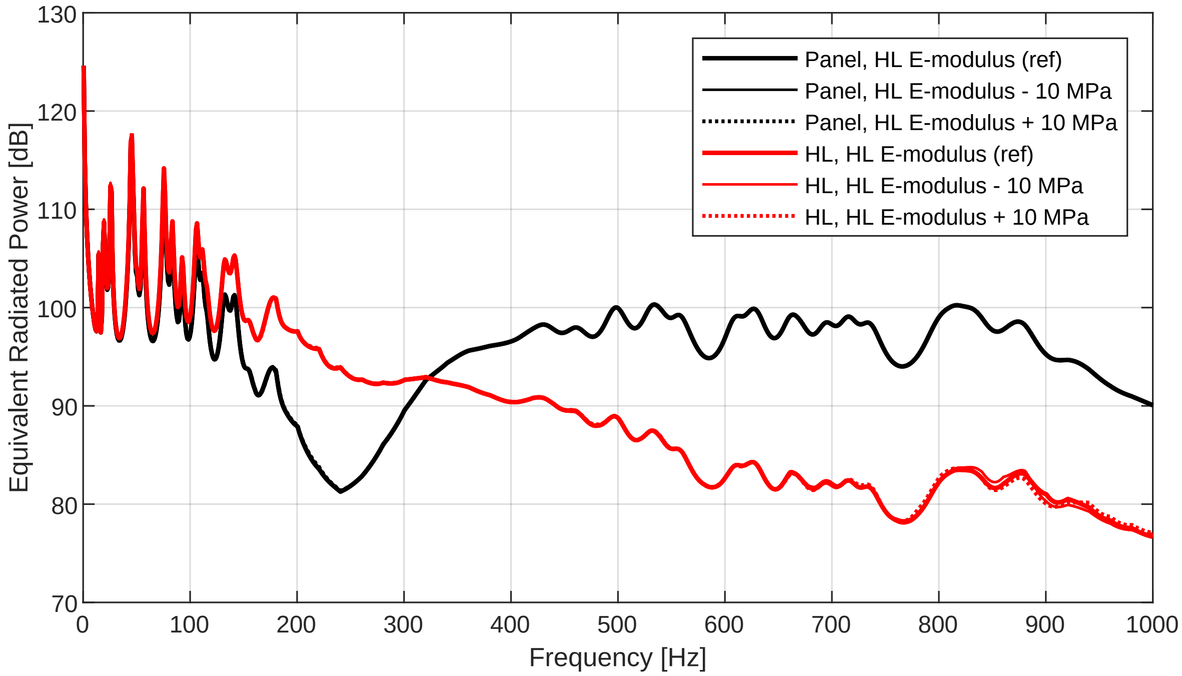

Figure 5.12: ERP response when Young's modulus of the HL was varied by ±10 MPa.

The stiffness of the HL, when varied by ±10 MPa, has a very small effect on the response of the system, except a slight deviation in the HL curve between 825 Hz and 1000 Hz.

5.4.5 Biot Parameters

A study regarding the Biot parameters, refer back to Table 4.3, was carried out to understand if a slight deviation in the parameter values would influence the ERP response. The following Biot parameters were considered:

- Porosity: Fraction between the pore volume and the total volume
- Tortuosity: Ratio between the actual path length considering the pores and the linear length
- Viscous characteristic length (VCL): Connection length between pores
- Thermal characteristic length (TCL): Pore diameter

The results are shown in Figures 5.13 to 5.16.

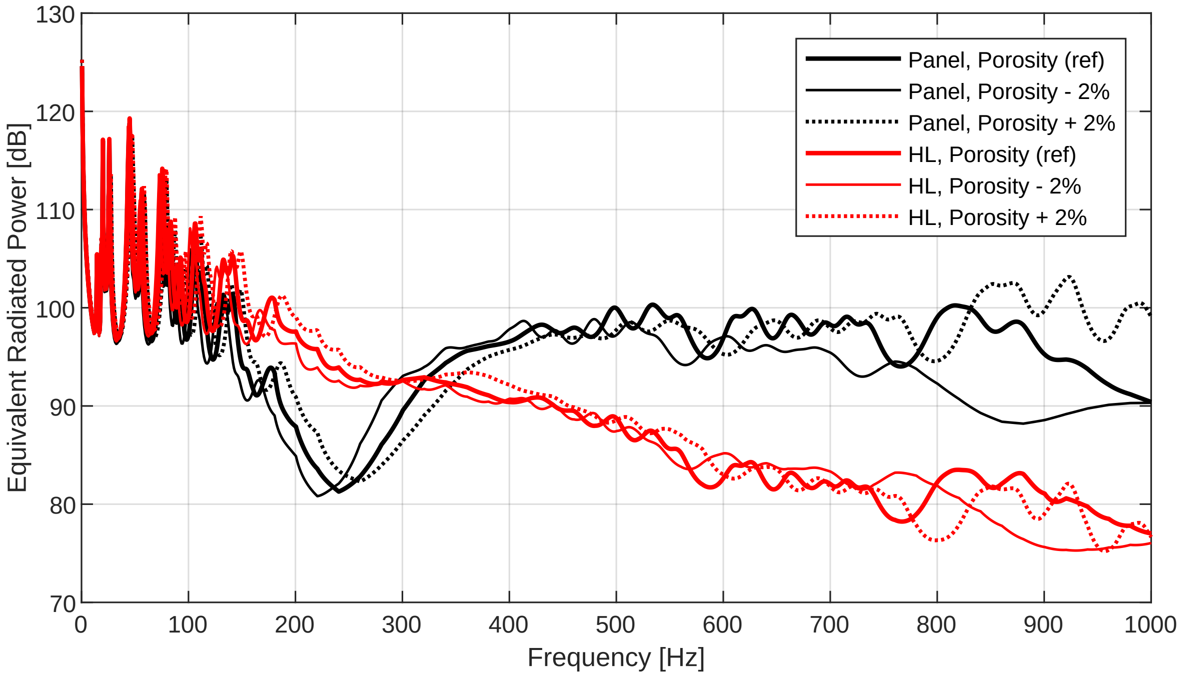

Figure 5.13: ERP response when the reference porosity value of the foam was increased and decreased with 2% porosity.

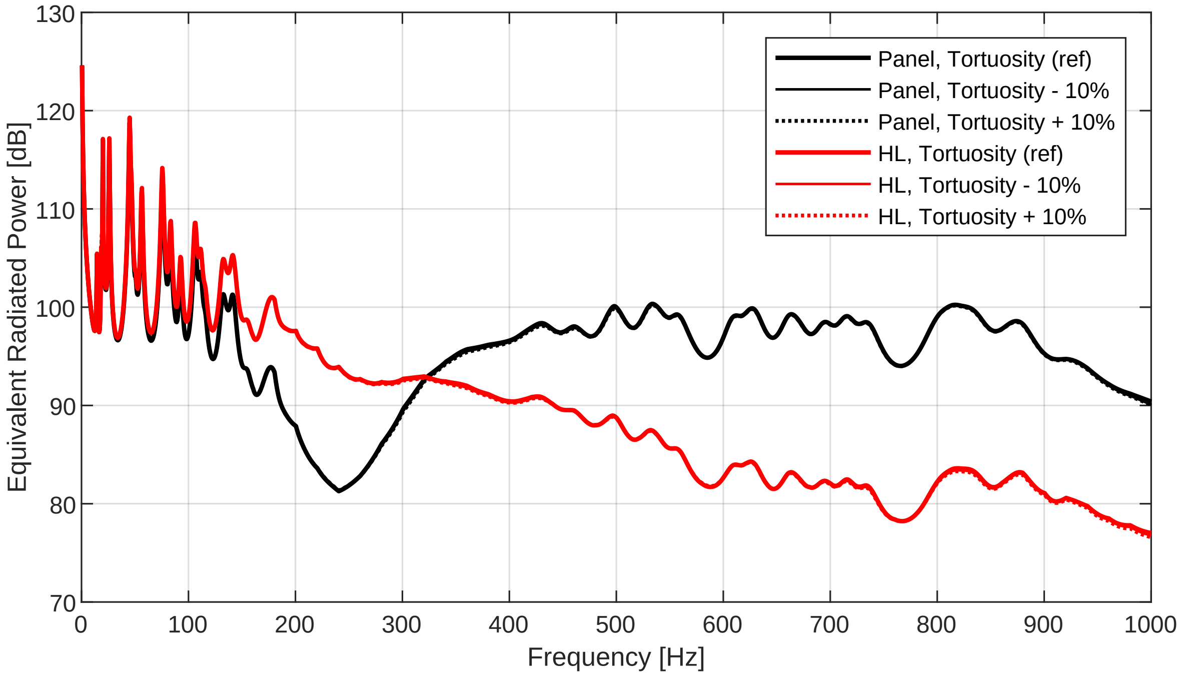

Figure 5.14: ERP response when the tortuosity of the foam was varied by ±10% relative to the reference tortuosity value.

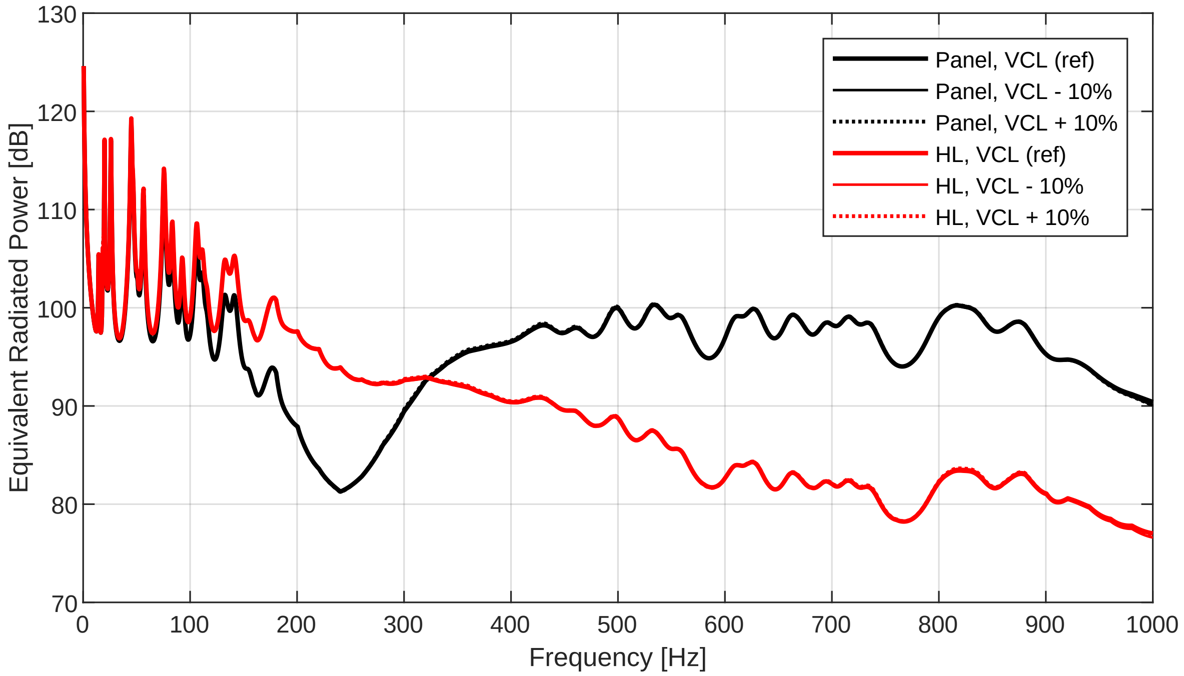

Figure 5.15: ERP response when the VCL was varied by ±10% relative to the reference VCL value.

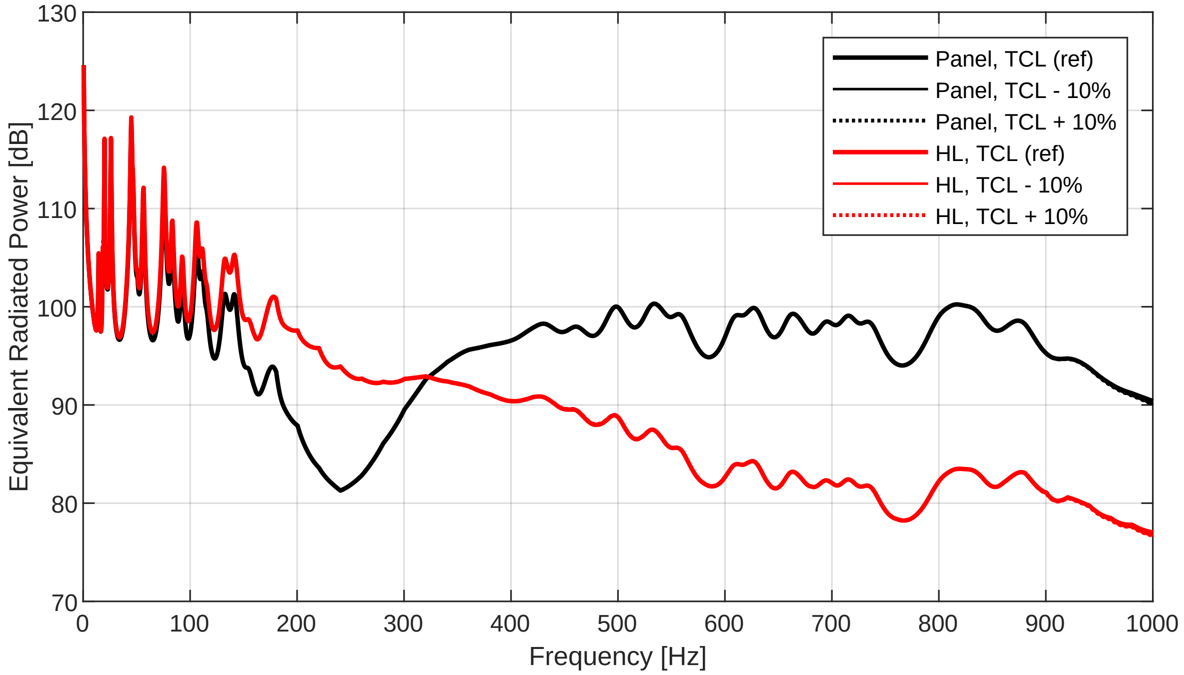

Figure 5.16: ERP response when the TCL was varied by ±10% relative to the reference TCL value.

The Biot parameter that has the biggest impact on the ERP data is the porosity of the foam. The porosity is directly related to the amount of solid material, which in turn affects the stiffness, mass and damping of the foam when considered as a continuum medium. As can be seen in Figure 5.13, the model with increased porosity has significantly larger amplitudes compared to the model with decreased porosity. The tortuosity, VCL and TCL were all varied by ±10% and the influence on the ERP was close to none.

Chapter 6

Simulation of Acoustic Radiation

The acoustic radiation from the NSM, LE and PEM models was simulated using modal frequency response analysis in MSC Nastran. The frequency range was limited to 100 – 600 Hz which accommodates the size of the acoustic domain and its FE mesh, but also covers all the three distinct regions for the vibration response as depicted in Figure 5.2. In the following chapter, the acoustic radiation is presented and visualized in the form of sound pressure using dB scale with a reference value of 2e-12. The results presented in this chapter concern a microphone positioned 900 mm above the setup as it is to represent the location of the passenger's hearing and is of most relevance when evaluating the acoustic response of the panel–carpet setup. After comparing the acoustic response of the different models to their respective vibration response presented in the previous chapter, it was deemed necessary to develop a fourth model that is based on the LE approach but has an equivalent acoustic medium for the foam, similar to the PEM model. Further, different ways of coupling the structure and the acoustic fluid were studied in order to investigate the physical phenomena that govern the sound radiation process.

6.1 Acoustic Radiation

Figure 6.1 shows the obtained acoustic pressure for the NSM, LE and PEM models at a distance of 900 mm above the panel–carpet setup. Unlike the vibration response where similarities could be observed among the models in the studied frequency range, it is safe to state that the different modelling approaches generally give different results regarding acoustic pressure. When performing the acoustic analyses, the vibration response was re-computed for each of the models to ensure that the implemented acoustic domain did not interfere with the ERP levels of the models. It turned out that when implementing an acoustic domain around the PEM model, the vibration response of the PEM model showed great deviation from the original curve seen in Figure 5.1. A number of studies concerning different ways of coupling the HL and foam in the carpet of the PEM model to the surrounding acoustic domain were performed, all of which resulted in deviating ERP curves – details can be found in Appendix A.

As the PEM model was deemed less credible when evaluating the acoustic response, there was a need to develop an LE model with an equivalent acoustic medium. This new model can be seen as a combination of the LE and PEM approaches, where the carpet was modelled based on the LE approach, but was supplemented with an internal fluid in the foam, here referred to as acoustic elements, to acknowledge the fact that air as well as acoustic waves can penetrate through the porous carpet. Hence, two separate domains – structural and fluid – were used in the new LE model instead of the Biot material in the PEM model.

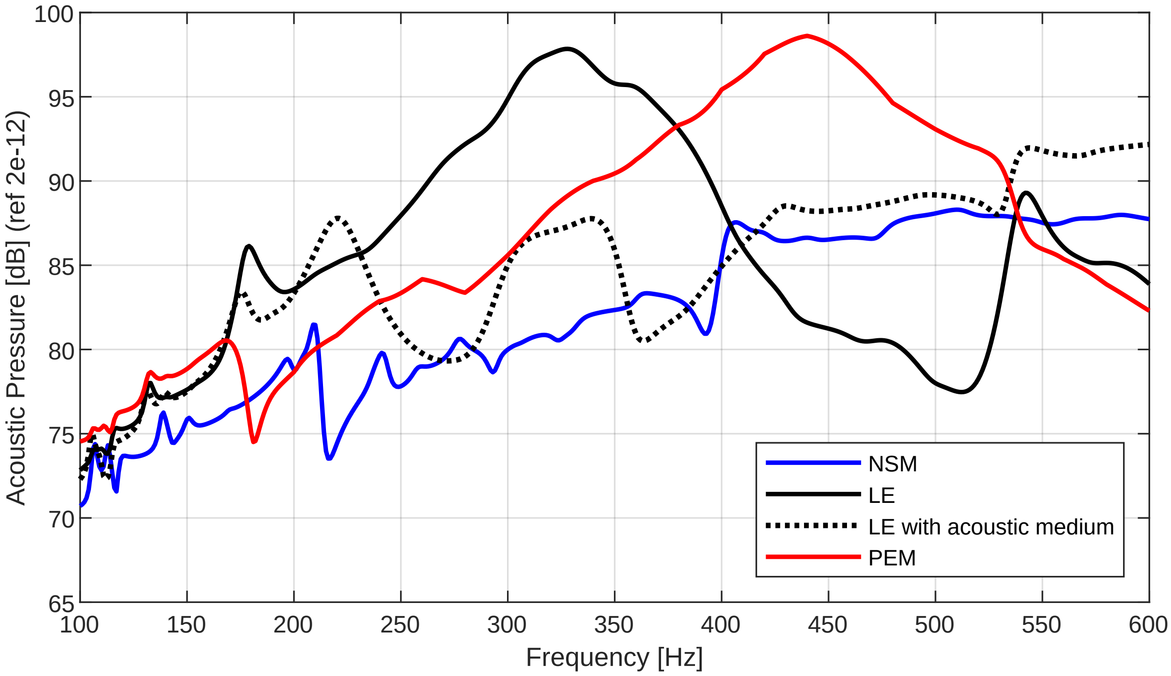

Figure 6.1: Acoustic pressure for the NSM, LE, and PEM models of the carpet, as well as the new LE model with acoustic medium, 900 mm above the panel–carpet setup.

Below follow observations made on the acoustic behaviour of the FE models with reference to the vibrational behaviour reviewed in Chapter 5:

- NSM model: In the lower end of the studied frequency range, the NSM model shows somewhat similar behaviour to that of the other models where an increase in the acoustic pressure curve can be observed. There is however an amplitude difference between the NSM model and the rest. This amplitude difference most likely stems from the fact that the acoustic waves radiating from the panel in the NSM model, have a longer distance to transfer to the microphone compared to the other models. When comparing to the ERP curves in Figure 5.1, this is the end of the range in which NSM starts to deviate from the LE and PEM models. Beyond this range, the NSM model in Figure 6.1 shows a completely different behaviour regarding acoustic response when compared to the other models. In the higher end of the studied frequency range, somewhat constant acoustic pressure can be observed.
- LE model: The acoustic response of the LE model has several similarities to its corresponding ERP curves in Figure 5.1. At about 180 Hz there is a local peak in acoustic pressure, which is the frequency at which the panel and the HL start to deviate from one another in the ERP curve. In the frequency range 180 – 325 Hz, the LE model shows a steady increase in acoustic pressure leading

to a global peak, after which a steep decline follows. When comparing to the vibrational behaviour illustrated by the corresponding ERP curves, this is the range at which the carpet reaches resonance and then declines gradually only to get vibration-isolated at higher frequencies. The downside of this model, however, is the fact that acoustic waves stemming from the panel vibration can not penetrate the carpet as the model lacks an internal fluid. It was therefore believed that the acoustic response of this model primarily reflects the vibrational behaviour of the HL as it is directly coupled to the external fluid above the setup.

- LE model with acoustic medium: At the lower end of the studied frequency range, more specifically 100 – 170 Hz, the LE model with acoustic medium shows similar behavior to the LE model without acoustic medium. This indicates that implementing an equivalent acoustic medium would not be necessary in this range as the presence of acoustic elements does not seem to affect the acoustic pressure of the model. This leads to believe that at lower frequencies, it is mainly the HL that contributes to the acoustic performance of the setup, as the purpose of adding acoustic elements in the foam is to enable acoustic waves originating from the panel to penetrate through the carpet and onto the external fluid. This hypothesis is further investigated in Section 6.3. Beyond 170 Hz, a continuous increase and decrease in the acoustic pressure can be observed up to about 430 Hz – which for instance marks the end of the second region in Figure 5.2. A clear correlation between the acoustic behaviour of this model and the ERP curves was hard to draw – however, it is of importance to note that this is a complex region in which the HL resonates, and vibrates in a conflicting pattern relative to the panel throughout this range; refer back to the ODS analysis in Section 5.2. Therefore, one possible explanation as to why the acoustic pressure curve of this region increases and decreases continuously is due to conflicting acoustic waves transmitted from the HL and the panel through the common acoustic medium, that amplify and cancel out each other repeatedly.
- PEM model: This model was deemed less credible for acoustic radiation after showing deviating ERP curves when the external acoustic domain was implemented.

In conclusion, the LE model with acoustic medium was believed to be the most accurate and reliable model as it enables acoustic waves to penetrate the porous carpet, and therefore acknowledges the sought physical phenomena. The decisive factor for this conclusion is the fact that the LE model without an acoustic medium for the foam is flawed acoustic–wise, as it can not reflect the true contribution of the panel to the overall acoustic radiation of the setup. Further, the PEM model was excluded from further studies after detecting deviating ERP curves.

6.2 Structure–Fluid Coupling in Porous Elastic Material Approach

It was suspected that the air within the porous elastic material in the PEM model did not couple correctly to the surrounding external fluid. In order to examine this hypothesis, the effects of the connection between the acoustic elements of the LE model (internal fluid in the foam) and the surrounding acoustic fluid (external fluid), along the sides of the carpet that are exposed to air, was investigated. The PEM approach was compared to the LE model with acoustic medium, with and without the connection between the two acoustic domains at the sides of the carpet. The results are shown in Figure 6.2.

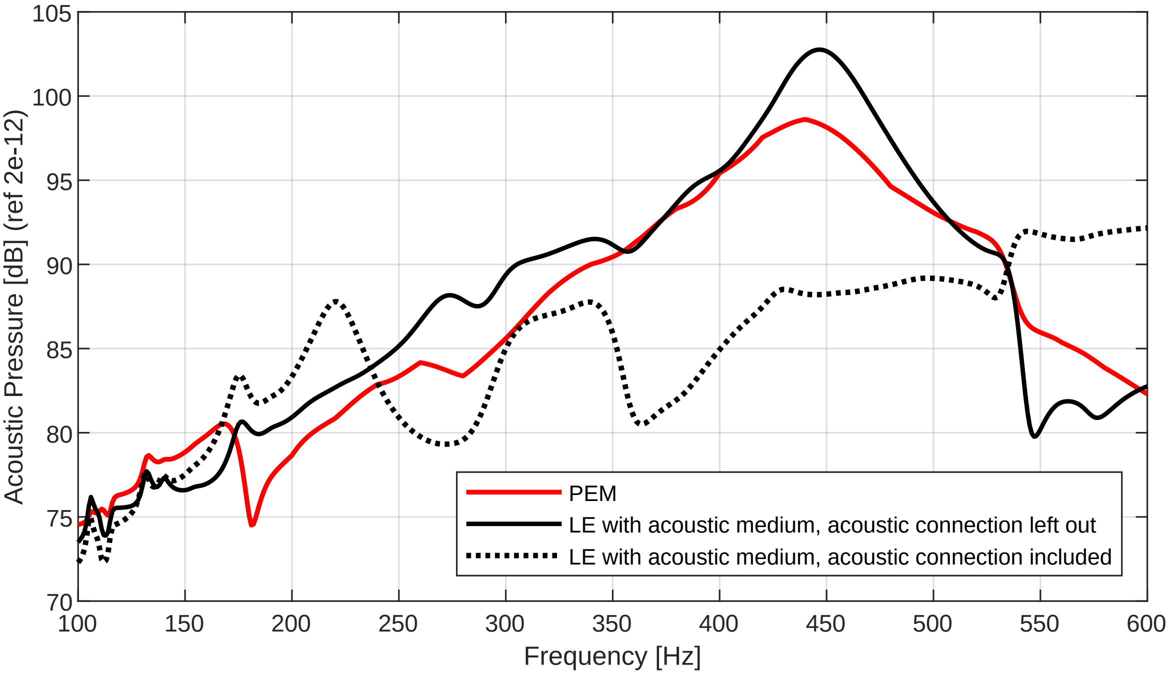

Figure 6.2: Acoustic pressure for the PEM model and LE model with acoustic medium. The effect of neglecting the connection between the acoustic elements and surrounding fluid in the latter is shown.

As clearly can be observed in Figure 6.2, the PEM and LE models show similar behaviour when the acoustic connection at the sides of the carpet in the LE model is left out, which clearly is an erroneous assumption. This confirms that the PEM approach in MSC Nastran results in a closed acoustic domain at the common interface of the foam of the carpet and the surrounding fluid. The results seen in Figure 6.2 highlights the importance of imposing correct structure–fluid coupling at the sides of the carpet.

6.3 Noise Radiation Process

Different ways of coupling the structure to the surrounding fluid were carried out to better understand the physical phenomena that govern the sound radiation process at different frequency ranges. There are mainly two sources to the structure–borne noise of the panel–carpet setup, see Figure 6.3:

- HL radiation: The vibrations of the panel are transmitted to the HL, which in turn gives rise to acoustic waves that propagate into the surrounding acoustic fluid.
- Panel radiation: The vibrations of the panel give rise to acoustic waves that propagate into the surrounding acoustic fluid. The acoustic waves, however, have to pass through the carpet before reaching the external fluid, which may result in transmission loss along the way.

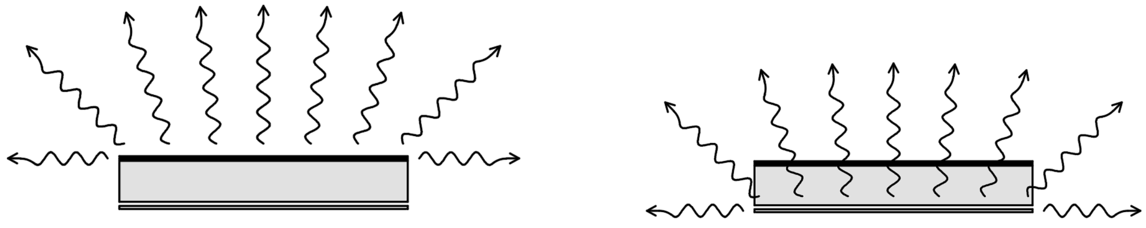

(a) HL radiation. (b) Panel radiation.

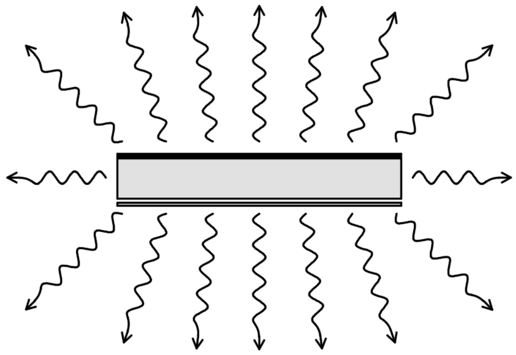

(c) Whole carpet radiation.

Figure 6.3: Illustration showing which interfaces of the structure were coupled to the surrounding fluid in order to capture the HL radiation, the panel radiation and the whole carpet (total) radiation.

In order to study the contribution of the HL and the panel to the total acoustic radiation of the setup, one source of radiation was treated at a time, while suppressing the other source. It was argued that the LE model with acoustic medium would be the most suitable model to perform this analysis on, as it theoretically would be able to capture all the relevant phenomena due to the presence of the acoustic elements in the foam of the carpet. Figure 6.4 shows the HL radiation and panel radiation, taking into account transmission loss, in relation to the total acoustic radiation of the setup shown earlier in Figure 6.1.

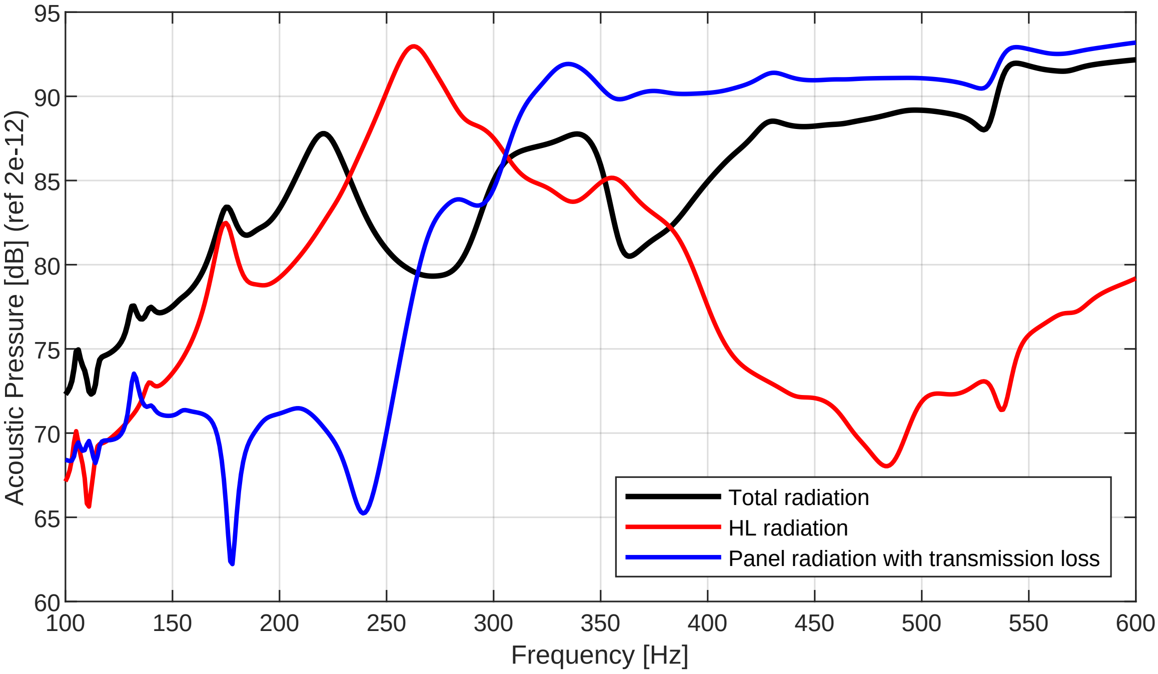

Figure 6.4: Acoustic radiation of the panel–carpet setup broken down into HL radiation and panel radiation, performed on the LE model with acoustic medium.

The transmission loss of the panel radiation was evaluated by introducing a fictitious second HL, only coupled to the surrounding fluid, which acts as an acoustic filter. This way, the acoustic waves stemming from the vibrations of the panel and transmitted through the acoustic medium, have to pass through the fictitious HL in order to spread to the external fluid above the setup. Figure 6.5 shows the panel radiation with and without transmission loss due to the presence of the HL. As can be seen in the figure, both curves show similar behaviour with a maximum amplitude difference equal to 5 dB at about 340 Hz. Further, it can be observed that the transmission loss due to HL is minimal in the frequency range 240 – 300 Hz, which for instance marks the range at which the ERP of the panel increases considerably; refer back to Figure 5.1.

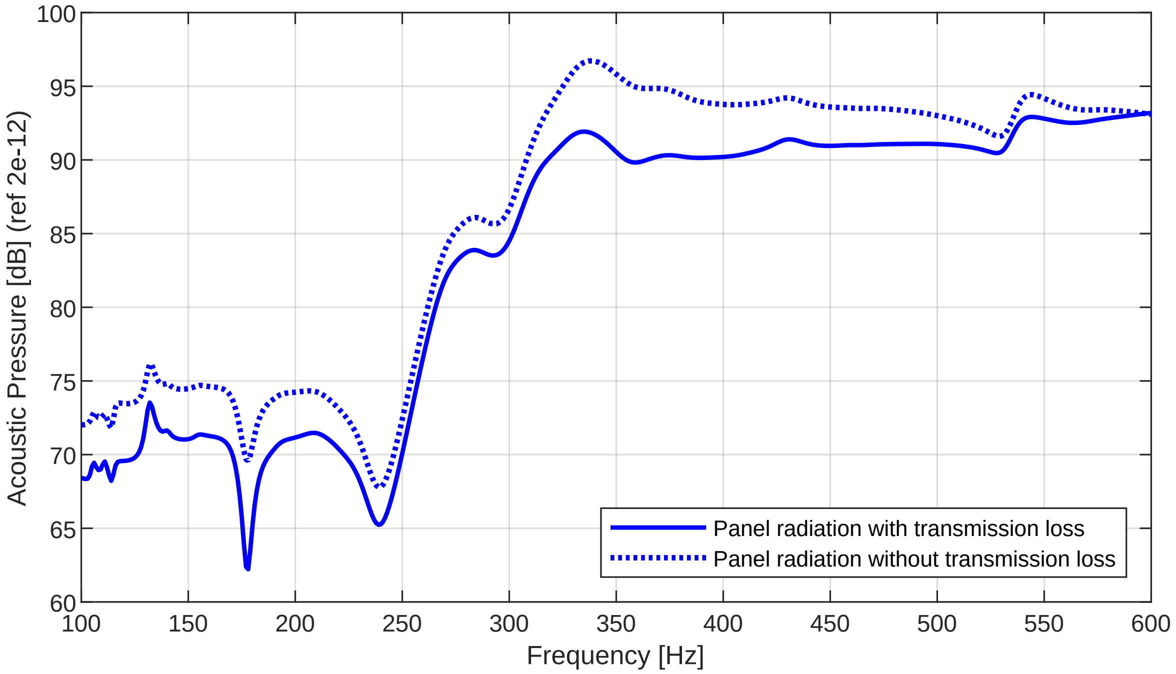

Figure 6.5: Effect of the transmission loss due to the presence of HL when acoustic waves arising from panel vibrations spread to the external fluid.

Looking back at Figure 6.4, the noise radiation process and the contribution of the HL and panel can be explained by breaking down the total radiation of the setup into HL radiation and panel radiation. In the lower end of the studied frequency range, where the panel and the carpet vibrate in a uniform manner, the HL and panel radiation curves demonstrate similar behaviour, indicating that the HL and the panel contribute to the acoustic performance of the setup equally. Beyond this range, it becomes clear that the main source of the structure–borne noise stems from the HL as the panel radiation remains rather constant with a few dips whereas the HL radiation increases to reach a peak at about 240 Hz. At the frequency range 240 – 430 Hz, the main source of the structure–borne noise becomes less obvious as the curves representing the HL and panel radiation switch behaviour. This is once again a rather complex region in which the governing physics are not as apparent as in the lower or higher end of the frequency range. By evaluating the ODS in this frequency range, refer back to Section 5.2, it is apparent that the panel and HL vibrate in opposite directions. This leads to believe that the acoustic waves propagating from the panel and HL counteract one another to some extent. Beyond 430 Hz, the panel radiation converges towards the curve representing the total radiation of the setup, whereas the HL radiation drops remarkably. It becomes evident that at higher frequencies, the main source of the structure–borne noise is the panel. This is confirmed by the fact that the carpet is vibration-isolated in this range, why its contribution to structure–borne noise is minimal.

Chapter 7

Experimental Testing and Correlation

Experimental testing of a flat floor panel and interior carpet setup, obtained from Volvo Cars and suppliers, was tested in free-free conditions. The testing was conducted at Volvo Cars laboratories in a semi-anechoic chamber to simulate free field conditions. A modal shaker was used in order to excite the setup with random noise for frequencies ranging from 0 to 1000 Hz. Accelerometers and microphones were placed to capture the vibrations of the setup along with the acoustic pressure, respectively. This chapter explains the testing methodology and reviews the obtained experimental results. Verification and correlation to numerical results follow at the end of the chapter. The reliability of the testing and possible sources of errors are also discussed.

7.1 Geometry and Material of Test Sample

A flat sample of a floor panel with the thickness 0.73 mm and the dimensions $390 \cdot 390$ mm^2 was tested along with an interior carpet of the same dimensions. The carpet is composed of 1.0 mm HL and a 25 mm foam, with material parameters according to Table 4.2 presented in Chapter 4 in this dissertation. No adhesives were used between the floor panel and interior carpet.

7.2 Experimental Setup and Methodology

The testing was performed in a semi-anechoic chamber in which the walls and the ceiling are covered with absorbent material, whereas the floor is made of concrete, see Figure 7.1. The purpose of an anechoic chamber is to not interfere with or affect sound propagation and radiation when acoustic measurements are performed, i.e. to simulate conditions similar to what is known as a free field. Since the floor of the laboratory is made of concrete, which is a reflective material, free field conditions were not fully obtained.

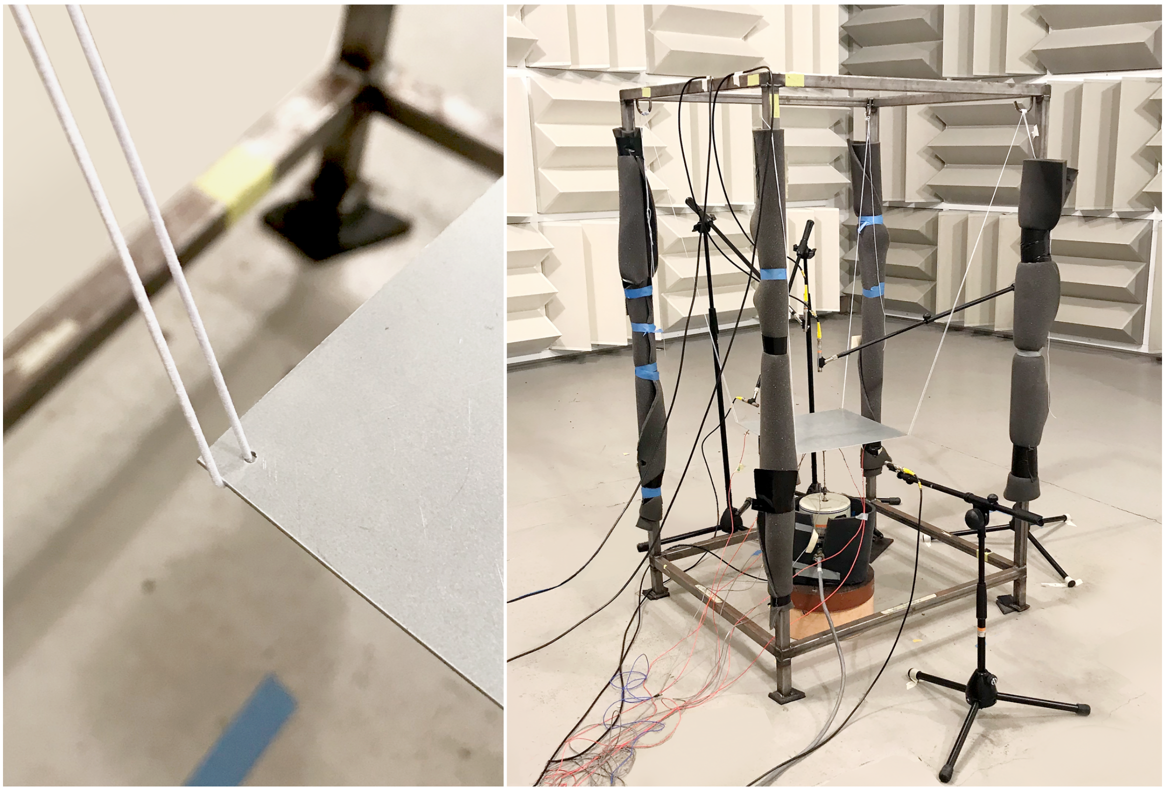

Figure 7.1: Laboratory setup. Left: 1.0 mm holes through which elastic bands were threaded to suspend the panel. Right: the rack used to suspend the panel. Conditions of the semi-anechoic chamber can be seen.

The floor panel was suspended horizontally using elastic bands attached to a rack. The elastic bands were threaded through 1.0 mm holes drilled at the corners of the panel. The use of elastic bands was thought to replicate free-free conditions as the bands do not restrain the movement of the panel and allow for rigid body modes with much lower frequencies than the flexible modes. Free-free conditions were however partially restricted as the suspended panel was attached to a modal shaker positioned underneath which acted as a support for the panel. Seven accelerometers were attached on the bottom side of the suspended panel to register the vibration of the panel, and four microphones were positioned nearby in order to perform acoustic measurements; see Figures 7.2 and 7.3 for a better understanding of the laboratory setup. This setup in which only the panel is suspended is hereinafter referred to as the base configuration. In addition to the base configuration, the interior carpet was placed on top of the panel in order to register the response of the panel–carpet setup. To capture the vibration response of the carpet, an eighth accelerometer was placed in the middle of the HL of the carpet. The position of the shaker, accelerometers and microphones is further reviewed in Table 7.1.

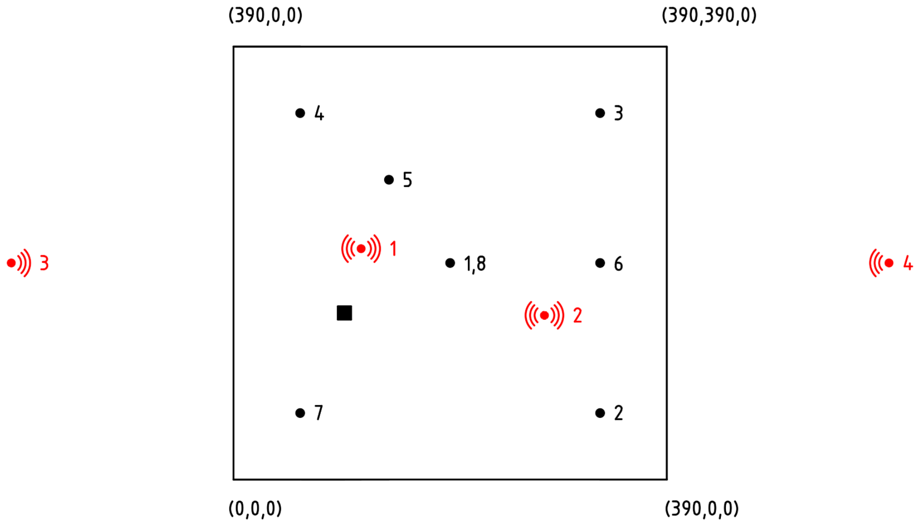
(390,0,0)
(390,390,0)
4
3
5
3
1
1,8
6
4
2
7
2
(0,0,0)
(390,0,0)

Figure 7.2: Laboratory setup seen from above. Accelerometers (black points) and shaker (black box) attached to the bottom side of the panel. Microphones represented by red points. Dimensions true to scale.

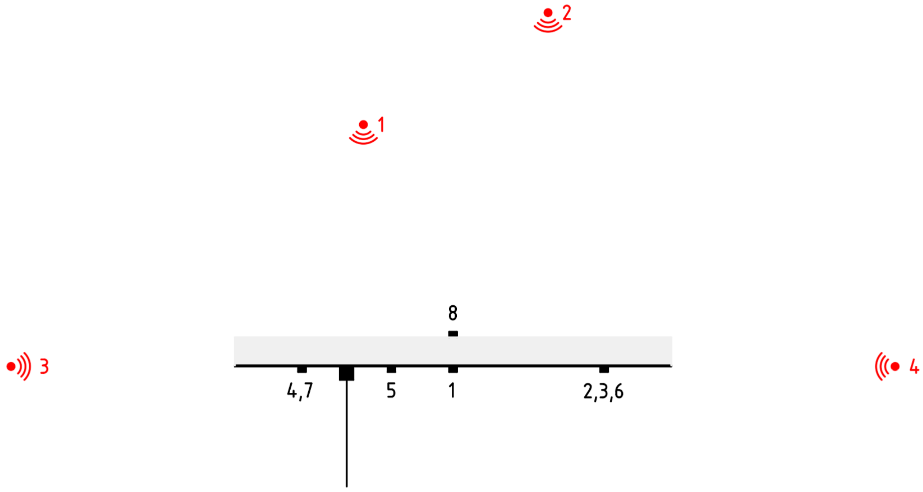
2
1
8
3
4
4,7
5
1
2,3,6

Figure 7.3: Laboratory setup seen from the side. Accelerometers (black points) and shaker (black box) attached to the bottom side of the panel. Microphones represented by red points. Dimensions true to scale.

	x coord. [mm]	y coord. [mm]	z coord. [mm]
Shaker	100	150	0
Acc 1	195	195	0
Acc 2	330	60	0
Acc 3	330	330	0
Acc 4	60	330	0
Acc 5	140	270	0
Acc 6	330	195	0
Acc 7	60	60	0
Acc 8	195	195	26
Mic 1	115	208	216
Mic 2	280	148	316
Mic 3	-200	195	0
Mic 4	590	195	0

Table 7.1: The position of the shaker, accelerometers and microphones. See Figure 7.2 for the origin of coordinates.

7.3 Measurement Results

Figures 7.4 and 7.5 show some of the registered accelerations and acoustic pressure of the base configuration with and without the interior carpet, when subjected to random noise by the modal shaker for a frequency range of 0 – 1000 Hz.

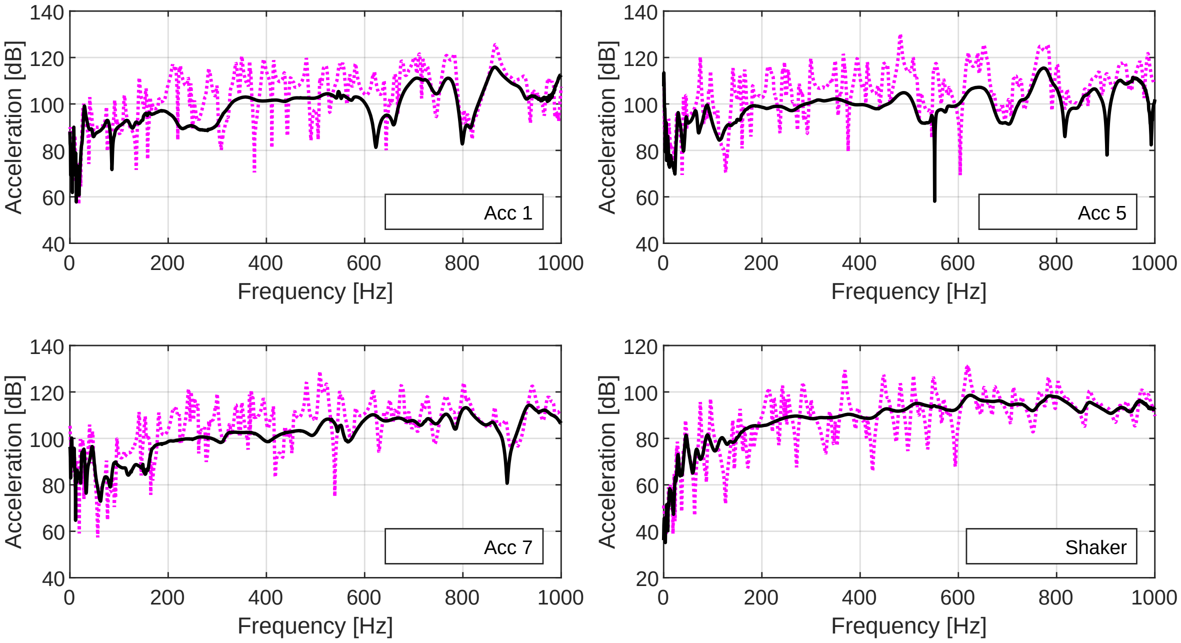

Figure 7.4: Registered accelerations of the base configuration (dotted magenta) as well as when the carpet is laid on top without any adhesives (black). For the rest of the accelerometers, refer to Appendix B.1.

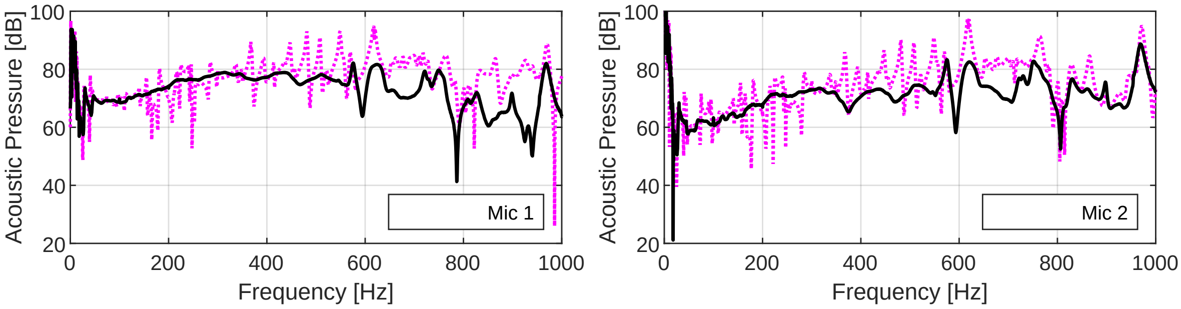

Figure 7.5: Registered acoustic pressure of the base configuration (dotted magenta) as well as when the carpet is laid on top without any adhesives (black). For the rest of the microphones, refer to Appendix B.2.

As can be observed in Figures 7.4 and 7.5, there is a clear advantage of using a carpet with HL on top of the panel, as it dampens out most of the resonance peaks seen in the accelerations and acoustic pressure of the base configuration. This damping effect is mostly pronounced in the frequency range 50 – 800 Hz. An interesting observation with regards to the higher frequencies is that the base configuration and the panel–carpet setup converges to an extent beyond 800 Hz, see especially Acc 1, Acc 7 and Mic 2. For the coherence of these measurements, refer to Appendix B.3.

7.4 Correlation to Numerical Results

A numerical FE model of the panel–carpet setup was developed based on the LE approach with acoustic medium for correlation purposes. To model the semi-anechoic chamber in which measurements took place, an acoustic domain similar to that of Section 4.5 was modelled. In order to account for the reflective floor, the bottom side of the sphere was cut and a rigid surface was assumed to simulate the reflective floor, see Figure 7.6. Microphones and accelerometers were placed in accordance with the actual positions in the laboratory setup, refer back to Table 7.1. The FE model was excited for a frequency sweep of 0 – 1000 Hz at the point where the shaker in the laboratory was attached.

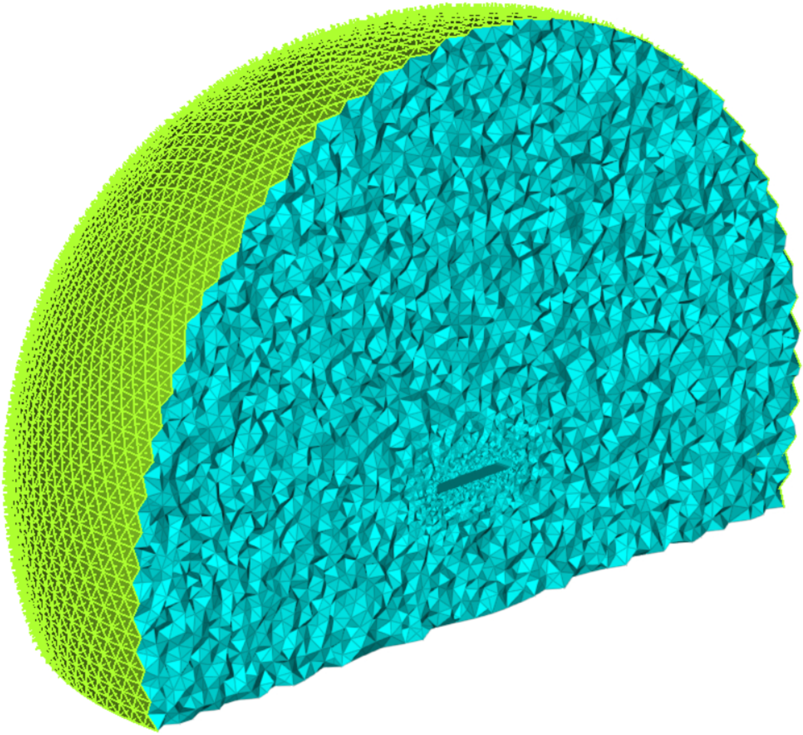

Figure 7.6: Acoustic domain representing the semi-anechoic chamber.

Figure 7.7 shows correlation between the measurements and numerical results for the acceleration response of the panel–carpet setup, whereas Figure 7.8 shows correlation of the acoustic response registered by Mic 1 and 2.

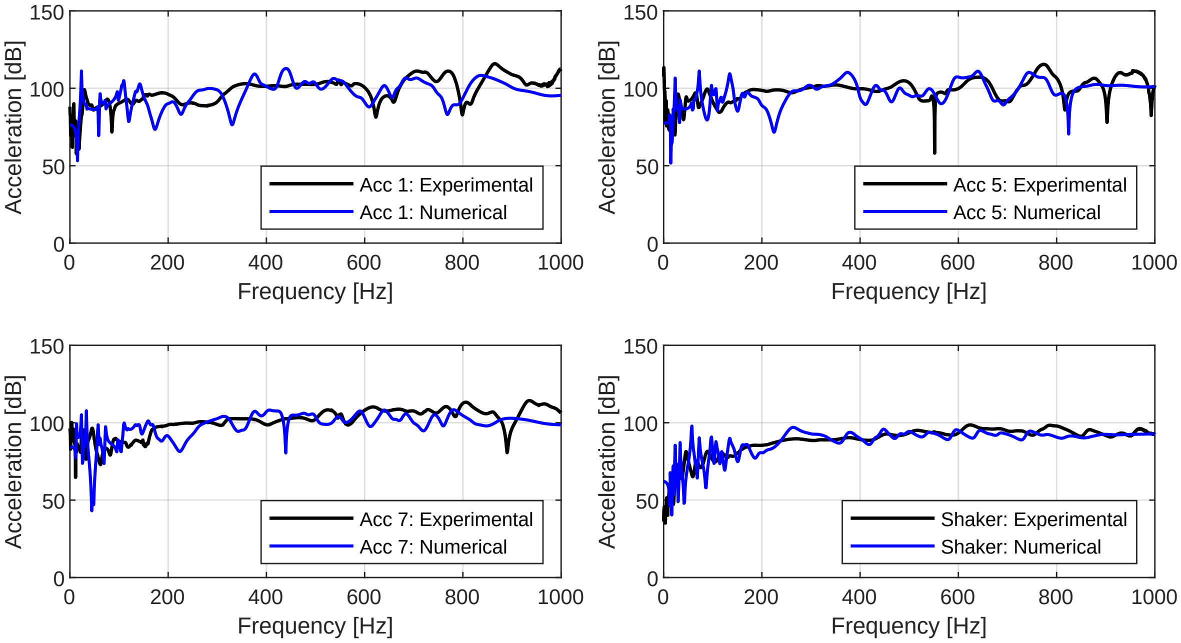

Figure 7.7: Correlation of acceleration response, registered by Acc 1, Acc 5, Acc 7 and the shaker for the panel–carpet setup to corresponding LE model. For coherence of the measurements, refer to Appendix B.3.

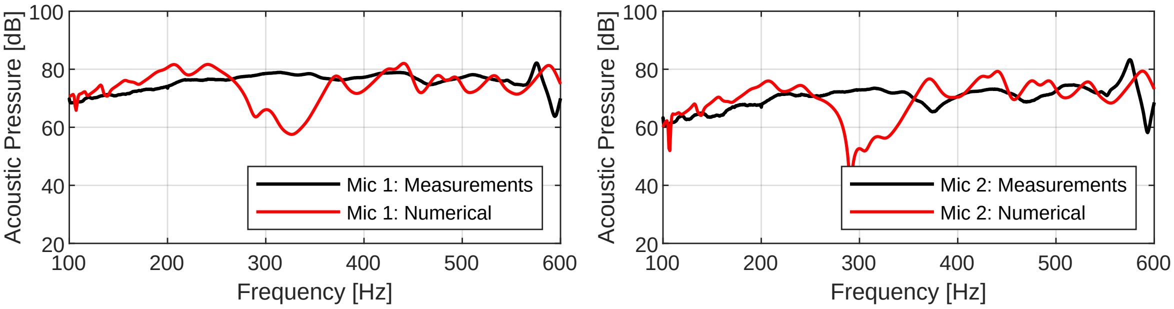

Figure 7.8: Correlation of the acoustic pressure, registered by Mic 1 and Mic 2, for panel–carpet setup to corresponding LE model with acoustic medium. For coherence of the measurements, refer to Appendix B.3.

As can be stated in Figure 7.7, the numerical and experimental data for the acceleration response correlates fairly well. However, the numerical results appear to have more acceleration peaks compared to the experimental data, suggesting that the assigned damping values in the FE model need to be adjusted. Considering the acoustic response seen in Figure 7.8, the numerical results correlate rather well to the measurements, with an exception for the frequency range 260 – 370 Hz. In this frequency range, a drop in the acoustic pressure of the numerical model can be observed. As mentioned previously, neither free-free conditions nor free field conditions were fully obtained, which might be a contributing factor for this deviation. Further, the size of the reflective floor in the FE model seen in Figure 7.6 might not fully represent the laboratory floor. Also, further modification of the damping of the FE model are likely to be needed as slight amplitude differences are seen at the lower and higher end of the studied frequency range. Since the numerical results follow the measurement data rather well, outside of frequency range 260 – 370 Hz, it can be seen as a verification of the observations and conclusions made in Section 6.3. It is to be noted that the frequency range 260 – 370 Hz coincides with the complex region mentioned back in Section 6.3, where the main contributor to structure–borne noise was harder to define.

Chapter 8

Conclusions and Discussion

This chapter presents conclusions and discussions based on the results presented in the dissertation. The aim of this dissertation was to provide a basis for rational design decisions for floor panel–carpet setups by investigating the noise radiation process and structure–acoustic interaction between vehicle floor panels and interior carpets. This was done by studying the FE analysis of the vibration response and acoustic radiation of a simplified panel–carpet setup with flat components, in which several FE models with different degree of complexity were used for the carpet. Experimental testing was also conducted for correlation and verification purposes.

8.1 Vibration Response

The following section summarizes the results and conclusions obtained in Chapter 5 in this dissertation. The observations concern the studied frequency range 0 – 1000 Hz.

8.1.1 Frequency–Dependent Behaviour

It was concluded that the panel–carpet setup exhibits different governing structural dynamic phenomena in different frequency ranges. Three regions with characteristic trends were marked in Figure 5.2, in which it was established that the carpet behaves as an added mass with no dynamic contribution to the setup in the first region below 120 Hz. In the second region, which extends from about 120 Hz to 430 Hz, a more complex behaviour of the panel and carpet was identified, in which vibrations of different amplitudes and of different directions between the panel and the carpet were observed due to internal resonances in the carpet. In the third region, beyond 430 Hz, it was confirmed that the carpet becomes vibration-isolated with low dynamic contribution to the panel vibrations.

8.1.2 Modelling Choice of Carpet

It was concluded that using the NSM approach is only valid for low frequencies, that is the first range marked in Figure 5.2. This is due to the mass effect which dominates within this range, which enables the carpet to be modelled as a pure mass put onto the panel. Beyond this range, it is not recommended to use the NSM approach as it gives false vibration response of the panel–carpet setup. Suitable options for modelling the carpet in the setup would be to use the LE or PEM approach which both gave similar results. Since the computational time for the PEM model was about three times the computational time for the LE model, there might not be a need to opt for the PEM approach when evaluating the vibration response of a panel–carpet setup.

8.2 Acoustic Radiation

The following section summarizes the results and conclusions obtained in Chapter 6 in this dissertation. The observations concern the studied frequency range 100 – 600 Hz.

8.2.1 Modelling Choice of Carpet

The acoustic radiation of a panel–carpet setup stems either from the vibrating panel or from the HL whose vibrations are transmitted from the panel. It was concluded that using the LE model up to about 170 Hz gave satisfactory results in relation to the LE model with acoustic medium. Beyond 170 Hz, it was argued that there is a need to supplement the carpet in the LE model with an internal fluid in order to enable acoustic waves stemming from the panel to penetrate the porous carpet. Further, it was observed that the NSM model gave similar results to the LE approach between 100 – 170 Hz, however with an amplitude difference. This amplitude difference could be due to the fact that the acoustic waves need to propagate through a longer vertical distance in the NSM model as no carpet is modelled. As the range 0 – 100 Hz was not studied, no conclusions regarding the behaviour of the NSM approach in relation to the LE approach can be stated. However, it is suspected that the NSM would be able to capture the acoustic radiation in low frequencies due to the previously discussed mass effect within this range. It was further observed that the use of the PEM approach led to doubtful results when studying the vibration response of the panel–carpet setup, why it was excluded from further analyses. As a concluding remark, it is recommended to use the LE approach with an implemented acoustic medium when performing acoustic analyses on a panel–carpet setup, in order to acknowledge the physical phenomena of interest beyond 170 Hz – the exact limit is case-specific.

8.2.2 Governing Physical Phenomena

It was concluded that the main contributor to structure–borne noise in the lower end of the studied frequency range is the HL, more specifically 120 – 240 Hz. This was for instance implied by the fact that supplementing the LE model with an acoustic medium did not affect the total acoustic radiation from the panel–carpet setup up to 170 Hz. At higher frequencies, 430 Hz and beyond, it was clear that the structure–borne noise primarily stems from the panel as convergence of the curves representing the panel radiation and the total radiation was observed, refer back to Figure 6.4. In the middle range, 240 – 430 Hz, no apparent statements can be made – however, it is suspected that both the panel and the HL contribute to the acoustic radiation with varying influence throughout the range. Further studies are needed to fully understand the governing physical phenomena and the main contributor to structure–borne noise within this complex region. It is of importance to note that the frequency ranges mentioned here regard the studied example case – however, the governing physical phenomena are expected to be the same as long the studied structure concerns a panel–carpet setup.

8.3 Experimental Testing and Correlation

This section summarizes the results and conclusions obtained in Chapter 7 in this dissertation. Experimental testing of a flat panel–carpet setup was conducted and verified by a numerical model based on the LE approach with an acoustic medium implemented in the carpet. The numerical results regarding the vibration response of the panel–carpet setup correlated well to the measurements. When evaluating the acoustic radiation, a clear correlation between the experimental and numerical results was observed at the lower and higher frequencies, refer back to Section 7.4. This gives credibility to the LE approach with acoustic medium as it was able to capture the acoustic response with fairly good accuracy in the said ranges, and can thus be seen as a verification of the findings presented in Section 8.2.2. Some deviation was observed within the frequency range 260 – 370 Hz, which once again is the complex region discussed through this work – implying that more research focused on this range should be carried out.

8.4 Proposals for Future Work

Below follow proposals for future work and suggestions for improvement, based on results and conclusions presented in this dissertation:

- Carry out further analyses for the complex region presented in this dissertation, that is 240 – 430 Hz, to better understand the noise radiation process when the panel and HL vibrate in counteracting manner.
- Implement the modelling techniques presented in this dissertation on a whole vehicle body with closed cavity, and evaluate the acoustic response with respect to a complete vehicle model. For instance, this can be performed by regarding the floor carpet on the body in white of a vehicle.
- The focus of future mobility development is moving towards energy efficiency and sustainability. Hence, optimizing the floor panel–carpet design becomes more relevant than ever. It is therefore of interest to perform a comprehensive design parameter study for the panel–carpet setup, and evaluate the vibration and acoustic response of the different designs. This could for instance include varying the material and/or thickness of the components of the panel–carpet setup. For this proposal, measurements of five additional interior carpets were performed – but not presented in this dissertation – for future correlation purposes.

Bibliography

[1] Jakob Dias Dos Santos Ingesson. Dynamic Analysis of the Interaction Between Vehicle Floor Panels and Interior Carpets – Simulations and Measurements. *TVSM-5000*, 2019.

[2] Arnaud Duval, Julien Baratier, Christian Morgenstern, Ludovic Dejaeger, Norimasa Kobayashi, and Hiroo Yamaoka. Trim FEM Simulation of a Dash and Floor Insulator Cut Out Modules with Structureborne and Airborne Excitations. *Journal of the Acoustical Society of America*, 123(5):3532, 2008.

[3] Christopher J Cameron, Per Wennhage, and Peter Göransson. Prediction of NVH Behaviour of Trimmed Body Components in the Frequency Range 100–500 Hz. *Applied Acoustics*, 71(8):708–721, 2010.

[4] Toru Yamazaki, Takashi Ono, Satoshi Utsumi, Kazuhito Misaji, and Minoru Kamata. Modeling of Floor Carpet on Vibration and Structure-Borne Noise Transmission. In *International Congress on Acoustics (ICA), Kyoto, Japan, Apr*, pages 4–9, 2004.

[5] John T. Katsikadelis. In *Dynamic Analysis of Structures*. Academic Press, 2020.

[6] Douglas Thorby. In *Structural Dynamics and Vibration in Practice*. Butterworth Heinemann, 2008.

[7] Dynamic Stiffness, Compliance, Mobility, and more... `https://community.sw.siemens.com/s/article/dynamic-stiffness-compliance-mobility-and-more`, 2019. [Online; accessed 30-03-2021].

[8] Mark Richardson and Ron Potter. Viscous vs. Structural Damping in Modal Analysis. In *46th Shock and Vibration Symposium*, volume 175. Citeseer, 1975.

[9] Peter Davidsson. *Structure-Acoustic Analysis; Finite Element Modelling and Reduction Methods*. Lund University, 2004.

[10] Håkan Carlsson. *Finite Element Analysis of Structure-Acoustic Systems; Formulations and Solution Strategies*. Lund University, 1992.

[11] Ola Flodén, Juan Negreira, Kent Persson, and Göran Sandberg. The Effect of Modelling Acoustic Media in Cavities of Lightweight Buildings on the Transmission of Structural Vibrations. *Engineering Structures*, 83:7–16, 2015.

[12] Göran Sandberg and Roger Ohayon. *Computational aspects of structural acoustics and vibration*, volume 505. Springer Science & Business Media, 2009.

[13] An Introduction to Transfer Path Analysis. `https://community.sw.siemens.com/s/article/an-introduction-to-transfer-path-analysis`, 2021. [Online; accessed 05-06-2021].

[14] ANSA pre-processor - BETA CAE Systems. `https://www.beta-cae.com/ansa.htm`, 2021. [Online; accessed 06-06-2021].

[15] MSC Nastran - Multidisciplinary Structural Analysis. `https://www.mscsoftware.com/product/msc-nastran`, 2021. [Online; accessed 06-06-2021].

[16] MSC Software. `https://www.mscsoftware.com/About-MSC-Software`, 2021. [Online; accessed 23-04-2021].

[17] BETA CAE Systems - META post-processor. `https://www.beta-cae.com/meta.htm`, 2021. [Online; accessed 06-06-2021].

[18] MATLAB - MathWorks - MATLAB Simulinks. `https://se.mathworks.com/products/matlab.html`, 2021. [Online; accessed 07-06-2021].

Appendices

Appendix A

ERP Deviation in Porous Elastic Material Approach

Figure A.1 shows the true ERP curve for the HL (solid red), as well as the deviating ERP when an acoustic fluid surrounding the PEM model was implemented (dotted red). Different combinations of the structure–fluid coupling conditions, SOPEN and SIMPER, were tested for a smaller frequency range of 200 – 280 Hz; all of which resulted in ERP curves that are far from the reference curve. The coupling condition SOPEN typically refers to porous material (e.g. foam), whereas SIMPER typically refers to impermeable material (e.g. HL).

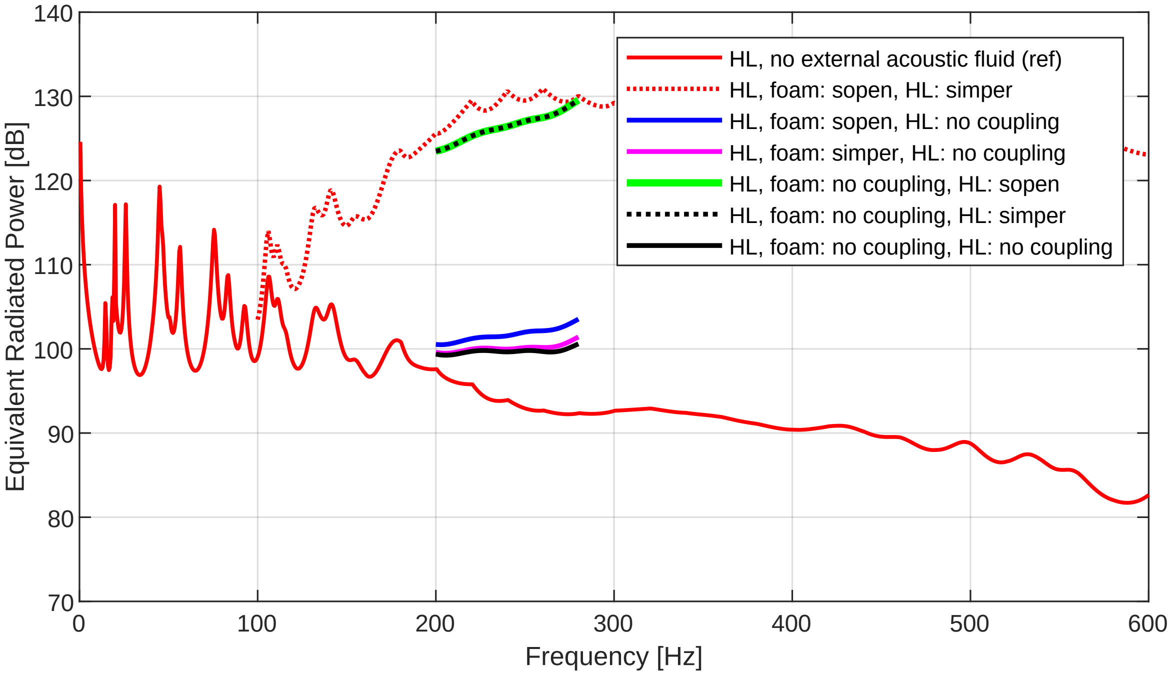

Figure A.1: Reference ERP curve of the HL using the PEM approach (solid red), along with deviating ERP curves due to the implementation of an external acoustic fluid domain.

Appendix B

Measurement Results

B.1 Acceleration

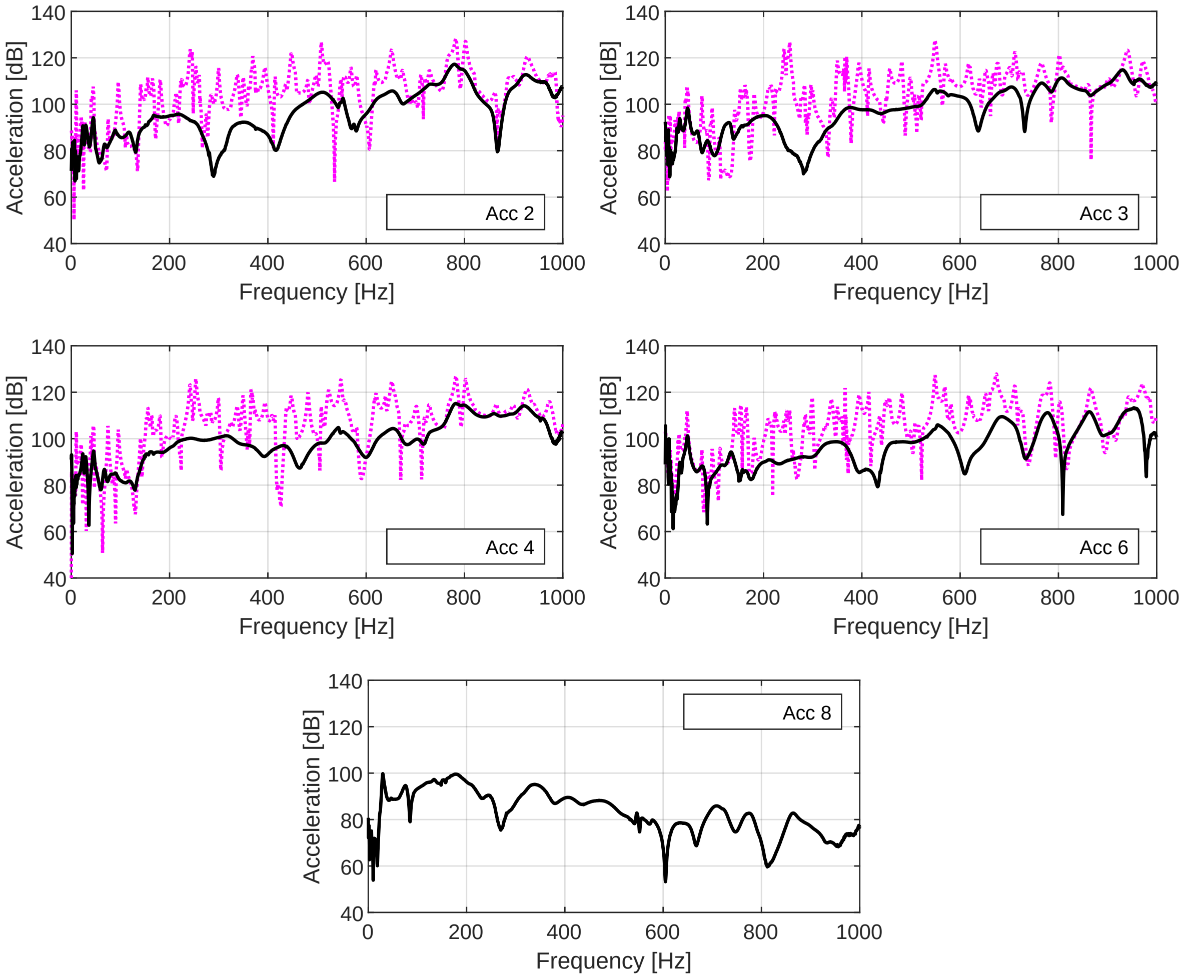

Figure B.1: Registered accelerations of the base configuration (dotted magenta) as well as when the carpet is laid on top without any adhesives (black). For Acc 1, Acc 5, Acc 7 and shaker, refer back to Section 7.3.

B.2 Acoustic Pressure

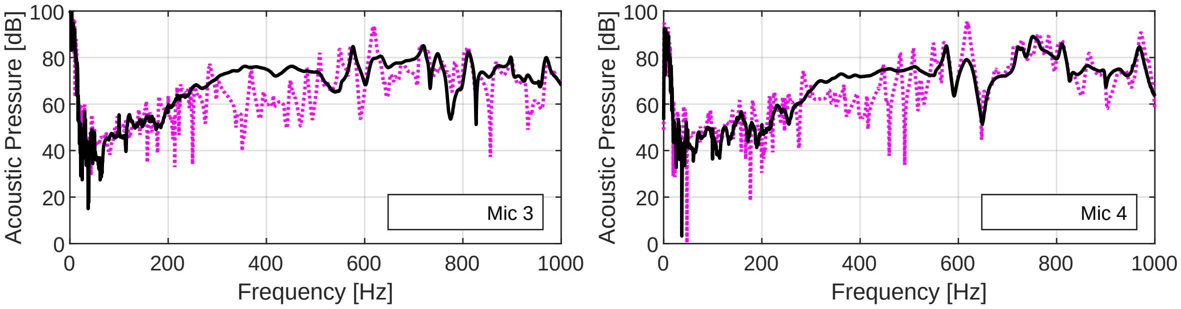

Figure B.2: Registered acoustic pressure of the base configuration (dotted magenta) as well as when the carpet is laid on top without any adhesives (black). For Mic 1 and Mic 2, refer back to Section 7.3.

B.3 Coherence

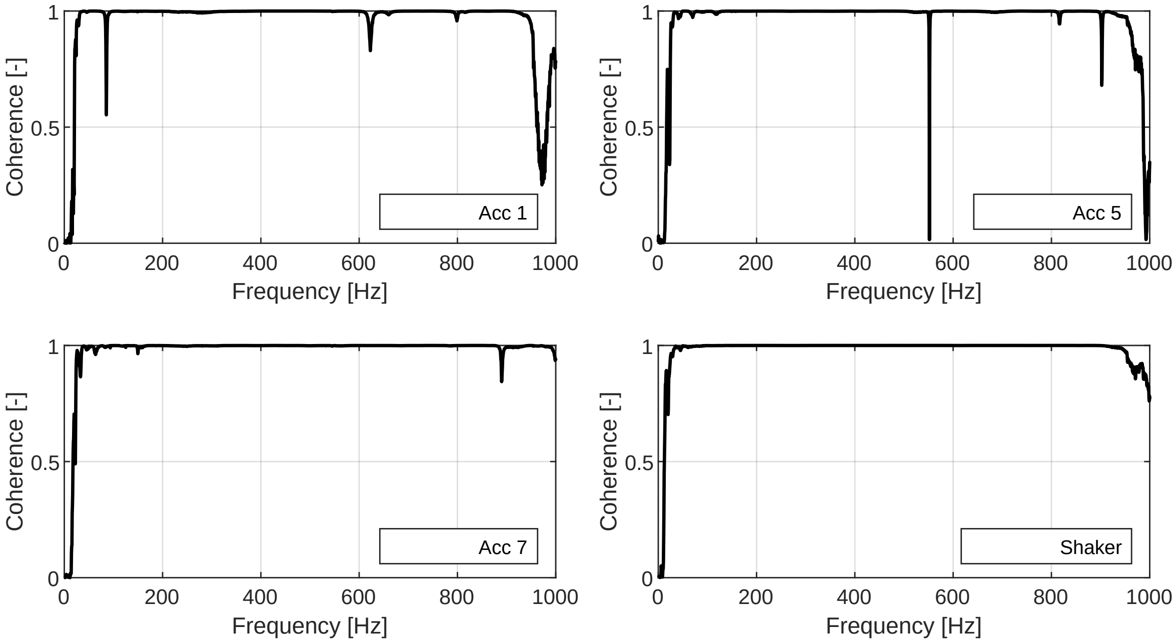

Figure B.3: Coherence of some of the registered accelerations of the panel–carpet setup. The measurement data was correlated to numerical results in Section 7.7.

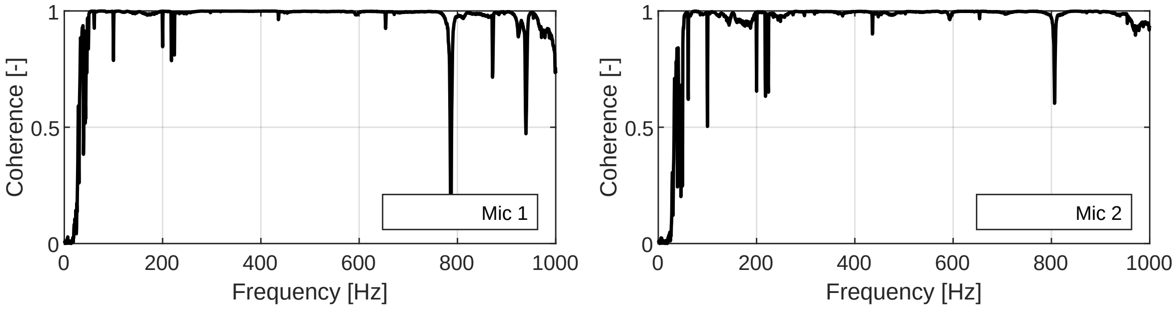

Figure B.4: Coherence of some of the registered acoustic pressure of the panel–carpet setup. The measurement data was correlated to numerical results in Section 7.7.